X-660-76-229

PREPRINT

THE SOLAR GAMMA RAY SPECTRUM BETWEEN 4 AND 8 MeV

R. RAMATY
B. KOZLOVSKY
A. N. SURI

OCTOBER 1976

GODDARD SPACE FLIGHT CENTER
GREENBELT, MARYLAND

The Solar Gamma Ray Spectrum

Between 4 and 8 MeV

R. Ramaty, B. Kozlovsky* and A. N. Suri**
Goddard Space Flight Center
Greenbelt, Maryland

*NAS-NRC Senior Resident Research Associate. Permanent Address: Physics Department, Tel Aviv University, Israel.

**Computer Sciences Corporation, Silver Spring, Maryland.

Abstract

We evaluate in detail the properties of nuclear gamma-ray emission in the 4 to 8 MeV range. This emission consists of broad ($\Delta E/E \sim 20\%$) and narrow ($\Delta E/E \sim 1\%$) lines resulting from nuclear reactions of energetic H, He, C and O nuclei with ambient matter. From the comparison of the calculations with observations of the 1972, August 4 flare we conclude: 1) that essentially all the observed radiation in the 4 to 8 MeV region is due to the superposition of broad and narrow lines of nuclear origin with almost no contribution from other mechanisms; 2) that the accelerated particles in the energy region from about 10 to 100 MeV/amu have a relatively flat energy spectrum (for a power law, E^{-s}, $s \leqslant 2.5$); 3) that the calculated gamma-ray spectrum obtained from an isotropic distribution of accelerated particles fits the observed spectrum better than the spectrum derived from an anisotropic distribution for which the particles' velocity vectors point towards the photosphere; and 4) that it is possible to set a stringent upper limit on the ratio of relativistic electrons to protons in flares, consistent with the small, but finite, electron-to-proton ratio in galactic cosmic rays.

I. Introduction

The solar gamma-ray spectrum from about 4 to 8 MeV consists of strong nuclear lines superimposed on continuum emission which could arise both from nuclear interactions and bremsstrahlung of energetic electrons. These nuclear reactions are almost exclusively due to interactions between hydrogen, helium, carbon, nitrogen and oxygen nuclei. Reactions due to energetic protons or alpha particles produce narrow lines with full widths at half maximum (FWHM) less than 150 keV; reactions caused by energetic C, N and O nuclei give rise to broad lines which in most cases cannot be distinguished from the continuum.

Line emission at 0.51, 2.2, 4.4 and 6.2 MeV and continuum emission extending up to about 7 MeV associated with the large solar flare of 1972, August 4 were reported by Chupp et al. (1973, 1975). These lines are due to positron annihilation, neutron capture by protons, and deexcitation of excited states in C and O (e.g. Ramaty, Kozlovsky and Lingenfelter, 1975). Electron bremmstrahlung could account for a significant fraction of the continuum, at least up to energies of several MeV (Suri et al. 1975; Bai and Ramaty 1976).

The production of gamma rays in solar flares has previously been studied by several authors (e.g. Lingenfelter and Ramaty 1967, Ramaty, Kozlovsky and Lingenfelter 1975, Crannell et al. 1976). Even though these papers provided detailed studies of the 0.51 and 2.2 MeV lines, they limited their treatments to only the gross features of gamma-ray production in the 4 to 8 MeV range. In particular, the shapes of the gamma-ray lines and the origin of the continuum in this energy band have not been investigated in detail. Ramaty and Crannell (1976) have provided a preliminary study of the shape of the 6.13-MeV line of ^{16}O and showed that

the mean energy of this line depends on the angular distribution of the primary energetic charged particles. They have limited their treatment, however, to the narrow line component only, whereas, as we shall show in the present paper, very important energy shifts do take place also in the broad components.

The purpose of the present paper is to provide a detailed treatment of nuclear gamma-ray production in the 4 to 8 MeV region. This energy band is of particular interest because it contains essentially all the lines of the abundant nuclear radiators, C and O, and conversely, it is not significantly populated by photons from other nuclei. Furthermore, as we shall show, the entire observed radiation in the 4 to 8 MeV range could be due to the superposition of broad and narrow lines from C and O with essentially no contribution from other radiation processes. This result allows us to carry out, for the first time, a detailed comparison between theoretical and astronomical gamma-ray line spectra.

In section II we examine in detail the nuclear cross sections. We find that the extant literature contains sufficient data to present a self-consistent picture for the reactions leading to gamma-ray production in the 4 to 8 MeV energy band. However, several key questions remain to be resolved. In particular, future experimental work, using existing laboratory accelerators and high resolution gamma-ray detectors should be able to resolve all the major lines in this energy band, and to provide information on the cross sections of several lines which have not been measured in past experiments using low resolution instruments. In Section III we use the nuclear cross sections to calculate the production of gamma rays, and we investigate the dependence of the shape of the gamma-ray lines on the energy spectrum and angular distribution of the primary accelerated charged particles. We use

detailed relativistic kinematics, and we take into account, whenever available, data on the angular distribution of the recoiling secondary particles. In Section IV we compare the results of our calculations with the observational data; in particular we present a direct comparison between the observed pulse-height spectrum and the calculated gamma-ray spectra folded through the response function of the University of New Hampshire gamma-ray detector flown on OSO-7. We apply the results of our calculations to solar flares, because until now no gamma-ray lines were convincingly observed from other astronomical sources. However, our results and techniques are relevant to future gamma-ray line observations from outside the solar system as well. We summarize our results in Section V.

II. Nuclear Cross Sections

The principal gamma-ray lines in the energy range from 4 to 8 MeV, their emission mechanisms and production modes are summarized in Table 1.

Line emission at 4.44 MeV is produced by the deexcitation of the first excited state of ^{12}C at 4.439 MeV and of the second excited state of ^{11}B at 4.444 MeV. Because of the recoil of the nuclei emitting gamma rays, the energies of the photons are 4.438 and 4.443 MeV respectively. The cross section for the reaction $^{12}C(p,p')^{12}C^{*4.439}$ MeV has been measured by Reich et al. (1956) between 5 and 5.7 MeV, by Barnard et al. (1966) between 6 and 11.5 MeV, by Conzett (1957) between 10 and 12 MeV, by Daehnick and Sherr (1964) between 14 and 19 MeV, by Dickens et al. (1963) between 18 and 30 MeV, by Stovall and Hintz (1964) at 40 MeV, by Fannon et al. (1967) at 49.5 MeV, by Horowitz and Bell (1970) at 100 MeV, by Emmerson et al. (1966) at 145 MeV, and by Tyren and Maris (1957) at 185 MeV. This cross section is shown by the solid line in Figure 1. We have used the average cross section at the resonances near the maximum at 10 MeV. However, we have not averaged the cross section at the resonance at 5.35 MeV since it may have some effect on the calculations for very steep particle spectra. The data points represented by the closed circles and square are based on measurements of gamma rays at 4.44 MeV resulting from the bombardment of C with protons (Zobel et al. 1968, Alard et al. 1974). The closed circle points were deduced by using the differential cross section at 135° given by Zobel et al. (1968) and their data on the angular distributions of gamma rays produced in proton bombardment of C. The data point of Alard et al. (1974) is already given in integral form. As can be seen, the gamma-ray data is consistent with the (p,p') data represented by the

solid line up to ~ 20 MeV. The discrepancy at higher energies is most likely due to the excitation of the 4.444 MeV level of ^{11}B by the reaction $^{12}C(p,2p)^{11}B$ which has an energy threshold of 22.1 MeV. This discrepancy cannot be due to the excitation of higher levels of ^{12}C which cascade to the 4.439 level because all the levels of ^{12}C above this level decay almost exclusively by particle emission (Ajzenberg-Selove and Lauritsen 1968). Since the kinematical widths of both 4.438 MeV and 4.443 MeV lines are ~ 50 keV, it is impossible to distinguish between these two lines. Therefore, in our calculations for the production of the 4.44 MeV line above 20 MeV we use the cross sections given by the dashed line in Figure 2. Up to about 100 MeV these cross sections are higher by approximately 25% than those used by Ramaty et al. (1975) who took into account only the (p,p') data, but they are lower than the cross sections given by Meneguzzi and Reeves (1975), because these authors assumed complete isotropy for the gamma-ray data of Zobel et al. (1968).

The cross sections for the reaction $^{12}C(\alpha,\alpha')^{12}C^{*}4.44$ MeV are given by the dashed-dotted line in Figure 1. The measurements of these cross sections were summarized in Ramaty et al. (1975). The open circle represents a measurement by Zobel et al. (1968) for 4.44-MeV gamma ray production in α-C interactions. As in the case of proton induced interactions, we interpret the difference between the gamma-ray data and the (α,α') data as due to the contribution of ^{11}B. In our calculations, we use the dashed-dotted line up to 5 MeV/amu and the dashed-crossed line at higher energies.

The 4.439 MeV level in ^{12}C and the 4.444-MeV level in ^{11}B can also be populated by spallation reactions on ^{16}O, as indicated in Table 1.

The cross sections for these reactions were taken from Zobel et al. (1968) and Alard et al. (1974), and are shown by the solid lines in Figure 2. For the $(\alpha,2\alpha)$ reaction we have only one experimental point at 13 MeV/nucleon. Our estimate of the cross section curve for this reaction is based on the expected behavior of the cross section near the threshold and an arbitrary extrapolation to higher energies where the contribution of this reaction is negligible in comparison with the proton induced reaction. Spallation reactions on ^{14}N can also lead to 4.44-MeV gamma-ray production. Using the measurements of Macleod and Reid (1966) at 13 MeV and those of Clegg et al. (1961) at 120 MeV, we estimate that the 4.44-MeV gamma-ray cross section from ^{14}N is larger than that from ^{16}O by about a factor of 2. With solar abundances, $N/O \sim 0.18$, the 4.44-MeV yield from ^{14}N is about 30% of the yield from ^{16}O.

Nuclear excitation of ^{16}O can produce several gamma-ray lines. The first excited state of ^{16}O at 6.05 MeV decays by $e^+ - e^-$ pair emission. The second, third and fourth excited states at 6.131, 6.919 and 7.119 MeV decay almost exclusively to the ground state producing gamma rays at 6.129, 6.917 and 7.117 MeV, respectively. The fifth excited state at 8.872 MeV decays 75% of the time to 6.131 MeV level and hence produces lines at 2.741 MeV and 6.129 MeV. Other transitions between the states of ^{16}O are also possible (De Meijer, Plendl and Holub 1974). In particular, excited levels at 10.94 and 11.07-MeV cascade to the ground state via the excited states at 6.131, 6.919 and 7.119 MeV with branching ratios given by Ajzenberg-Selove and Lauritsen (1968).

Gamma-ray lines from ^{16}O can also be produced by spallation reactions. The reaction $^{16}O(p,2p)^{15}N$ and $^{16}O(p,pn)^{15}O$ can populate excited states in

^{15}N and ^{15}O. The strongest lines from ^{15}N are at 6.322, 5.270 and 5.298 MeV and from ^{15}O at 5.180, 5.241 and 6.176 MeV.

The cross section for producing gamma rays at 6.129 MeV from proton interaction with ^{16}O is shown in Figure 3 by the solid line. This cross section is sum of the cross sections of the reaction $^{16}O(p,p')$ $^{16}O^{*}6.131$ and 75% of the cross section for the reaction $^{16}O(p,p')$ $^{16}O^{*}8.872$ and about 50% of the cross section of the reaction $^{16}O(p,p')$ $^{16}O^{*}11.07$. These cross sections were measured by Dangle et al. (1964) between 7 and 10.5 MeV, by Kobayashi (1960) between 11 and 15 MeV, by Daehnick (1964) between 15 and 19 MeV, by Hornyak and Sherr (1955) at 19 MeV, by Crawley and Garvey (1967) at 17.5 MeV, by Austin et al. (1971) between 17 and 45 MeV, and by Sundberg and Tibell (1969) at 185 MeV. Since the contributions of cascades from higher levels to the 6.131-MeV level was neglected by Lingenfelter and Ramaty (1967) and Ramaty, Kozlovsky and Lingenfelter (1975), the cross sections for 6.129-MeV line emission used by these authors were somewhat lower ($\sim$ 30-50% between 10 and 50 MeV) than those used in the present calculation.

There are no measurements of 6.129-MeV line emission from spallation reactions on ^{20}Ne. If we assume that the cross section for the reaction $^{20}Ne(p,p\alpha)^{16}O^{*}6.129$ is similar to that of the reaction $^{16}O(p,p\alpha)^{12}C^{*}4.439$ then, with solar abundances, the contribution of ^{20}Ne to 6.129-MeV emission is less than about 10% of the contribution of ^{16}O.

The data points shown in Figure 3 are based on the measurements of Zobel et al. (1968), Foley et al. (1962), and Alard et al. (1974). In these measurements the cross sections were determined by measuring gamma rays at about 6.2 MeV. Because of the poor energy resolution of the detectors used, these gamma rays include the lines at 6.129 MeV from

^{16}O, at 6.176 from ^{15}O and 6.322 MeV from ^{15}N. The difference between the dashed and solid lines in Figure 3 gives the sum of the cross sections for the production of the 6.176 and 6.322 MeV lines. This cross section is shown by the dashed-dotted line in Figure 2. There is only one direct high-resolution measurement of gamma rays from ^{16}O which can resolve the 6.129, 6.176 and 6.322-MeV lines (Goryachev et al. 1973). According to this measurement the 6.322-MeV line is stronger by about a factor of 2 than the line at 6.176 MeV. Assuming that this ratio holds also at lower energies, we take the cross sections for the production of the 6.322-MeV and the 6.176-MeV lines as 2/3 and 1/3, respectively, of the dashed-dotted curve in Figure 2. The sum of the cross sections for the reactions $^{16}O(p,pn)^{15}O^*$ and $^{16}O(p,2p)^{15}N^*$ leading to $\sim$ 5.2-MeV photons is shown by the dashed line in Figure 2 based on data by Zobel et al. (1968).

Most of the experimental measurements of the cross sections for the excitation of the 6.919 and 7.119 MeV levels in ^{16}O by (p,p′) reactions do not resolve these two levels. Therefore, in Figure 4 the solid line gives a fit to the sum of the cross sections for the excitation of these levels based on measurements of Zobel et al. (1968). Measurements of (p,p′) reactions to these levels by Kobayashi (1960) at 5.6 MeV and Crawley and Garvey (1967) at 17.5 MeV coincide with this line. At higher energies the measurements of (p,p′) reactions by Hornyak and Sherr (1955) and Sundberg and Tibell (1969) give lower values. The difference should be attributed to contributions of spallation lines such as the 7.3 MeV from ^{15}N, which show up at high energies.

The 2.741 MeV line is produced by transitions between the 8.87 MeV level

to the 6.13 MeV level in ^{16}O (branching ratio 76%). The dashed line in Figure 4 is based on the measurements of Crawley and Garvey (1967) at 17.3 MeV, and of Austin et al. (1971) between 17 and 45 MeV. The data points are from Zobel et al. (1968). These data are in agreement with the (p,p′) measurements. The $\alpha + {}^{16}O \rightarrow \gamma_{6.92+7.12}$ cross section is shown by the dashed-dotted line in Figure 4. This line is based on measurements of Corelli et al (1959) at 4.5 MeV/amu, of Harvey et al. (1966) at 10 MeV/amu and of Zobel et al. at 13 MeV/amu.

In the interval 4 to 8 MeV the interactions of protons with C produce a cluster of lines around 6.5 MeV due to deexcitations of excited states in ^{11}C and ^{11}B. These are populated by (p,pn) and (p,2p) reactions which are known to be important processes leading to spallation. The cross section for this cluster, as given by Zobel et al. (1968) and Clegg et al. (1961), is on the average about 1/4 of the cross section for the production of the $\sim$ 5.2-MeV feature from ^{16}O by the same type of reactions. We use this ratio in our subsequent calculations

III. Gamma-Ray Production

1. Total Narrow Line Production Rates

The instantaneous reaction rates between energetic protons or alpha particles and the ambient medium for the processes listed in Table 1 can be written as

$$q_i(p) = n_i \int dE\, \sigma_i(E) c\beta\, N_p(E) dE \qquad (\text{sec}^{-1}) \qquad (1)$$

and

$$q_i(\alpha) = n_i \int dE\, \sigma_i(E) c\beta\, N_\alpha(E) dE, \qquad (\text{sec}^{-1}), \qquad (2)$$

where n_i and σ_i are the target number density and cross section for

the particular reaction considered, E and cβ are energy per amu and velocity of the projectiles, and $N_p(E)dE$ and $N_\alpha(E)dE$ are tne total number of protons and alpha particles in the interaction region with energies per amu in dE around E. The instantaneous rates given by equations (1) and (2) are valid for both the thin and thick target models (e.g. Ramaty et al. 1975). The relationships between N_p and N_α and the source functions of these particles are different, however, in the two models.

We have evaluated equations (1) and (2) for the cross sections given in Section II, ambient abundances normalized to 1 H atom cm^{-3} by the ratios H:He:C:N:O = 10^4:10^3:3.7:1.2:6.8 (Cameron 1973, except for the He/H ratio) and for proton and alpha particle spectra of the form

$$N_p(E) = 10N_\alpha(E) = (s-1)30^{s-1} \times \begin{cases} E_c^{-s} & E \le E_c \\ E^{-s} & E \ge E_c \end{cases} . \qquad (3)$$

These spectra are normalized such that for $E_c \le 30$ MeV/amu and $s > 1$, the integral of $N_p(E)$ above 30 MeV is unity. We use power-law spectra with low-energy cutoffs, because, as we shall see below, significant changes in the gamma-ray spectra are caused by variations in the value of E_c.

The resultant production rates of narrow gamma-ray lines at the indicated energies are shown in Figure 5 as functions of the spectral index s and the cutoff energy E_c. The production rates of these narrow lines are due to the interaction of energetic protons and alpha particles with ambient C, N and O. The inverse reactions induced by energetic C, N and O nuclei leading to broad lines are not included in the curves in Figure 5.

The 4.44 curve of Figure 5 represents the sum of the 4.438 and 4.444-MeV lines listed in Table 1; the 5.2 curve is the sum of the 5.180, 5.298, 5.270 and 5.298 lines; the 6.13 curve represents the 6.129-MeV line; the

6.2 curve is the sum of the 6.176 and 6.322-MeV lines, but as discussed in Section II, the 6.322 line appears to be stronger than the line at 6.176 MeV; the 6.5 curve is the sum of the 6.337, 6.478, 6.741 and 6.791-MeV lines; and the 7 line is the sum of the 6.917 and 7.117-MeV lines.

As can be seen from Figure 5, the strongest line in the 4 to 8 MeV range is at 4.44 MeV. The ratio between its intensity and that of the next strongest line, at 6.13 MeV, is about 2, independent of s or E_c. The line at 6.32 MeV and the feature at $\sim$ 5.2 MeV, due to spallation reactions, are relatively strong for flat particle spectra, but become quite insignificant for accelerated particles with steep energy spectra.

The curves labelled q_p and q_α represent the sum of the production rates of the narrow lines listed in Table 1, due to proton and alpha particle interactions, $q_p = \Sigma\, q_i(p)$ and $q_\alpha = \Sigma q_i(\alpha)$. As can be seen, $q_p + q_\alpha$ equals to the sum of the production rates of the various lines shown in this figure.

2. Gamma-Ray Spectra

We proceed now to calculate the spectrum of gamma rays resulting from the above interactions by taking into account in detail the kinematics of the interactions. We first discuss the narrow gamma-ray lines resulting from the direct excitation reactions.

Consider the reaction between a proton or alpha particle of mass m_1 and energy per amu E, and a target of mass m_2 which is stationary in the frame of the Sun. This reaction leads to an excited nucleus of mass $m_3 = m_2 + \epsilon_x$, where ϵ_x is the energy of the excited level. The Lorentz factor (total energy per rest mass energy) of the excited nucleus in

the center-of-mass (c.m.) frame is given by

$$\gamma_s^* = (E_{cm}^2 + m_3^2 - m_1^2)/(2m_3E_{cm}), \tag{4}$$

where

$$E_{cm} = [(m_1+m_2)^2 + 2m_1m_2\ E/m_p]^{\frac{1}{2}} \tag{5}$$

is the total energy in the c.m. frame and m_p is the proton mass. In terms of this Lorentz factor and the directional cosine of the excited nucleus in the c.m. frame, μ_s^*, the Lorentz factor and directional cosine of the excited nucleus in the frame of the Sun are given by

$$\gamma_s = \gamma_c\ \gamma_s^* + \sqrt{\gamma_c^2-1}\ \sqrt{\gamma_s^{*2}-1}\ \mu_s^* \tag{6}$$

$$\mu_s = [\gamma_s^*\ \sqrt{\gamma_c^2-1} + \gamma_c\ \sqrt{\gamma_s^{*2}-1}\ \mu_s^*]/\sqrt{\gamma_s^2-1}, \tag{7}$$

where

$$\gamma_c = (E_{cm}^2 + m_1^2-m_2^2)/(2m_1E_{cm}) \tag{8}$$

is the Lorentz factor of the c.m.

We denote by μ_γ' the cosine of the angle between the gamma ray and the velocity vector of the excited nucleus in the rest frame of this nucleus. In the frame of the Sun this directional cosine is

$$\mu_\gamma = (\beta_s + \mu_\gamma')/(1 + \beta_s\mu_\gamma'), \tag{9}$$

where $\beta_s = \sqrt{\gamma_s^2-1}/\gamma_s$. Taking into account the Doppler effect and the recoil of the nucleus during photon emission, the gamma ray energy is given by

$$\epsilon_\gamma = \Delta\epsilon[1-\Delta\epsilon/(2Mc^2)]/[\gamma_s(1-\beta_s\mu_\gamma)], \tag{10}$$

where $\Delta\epsilon$ is the difference between the energies of the initial and final states of the transition and M is the mass of the gamma-ray emitting nucleus. Equation 10 is valid if the gamma ray is emitted while the nucleus is still

in flight. Only in solids will some nuclei stop before emitting photons. The astrophysical consequences of this possibility were discussed by Lingenfelter and Ramaty (1976). Finally, the cosine of the angle between the gamma ray and the velocity vector of the projectile is

$$\mu = \mu_s \mu_\gamma + \sqrt{1-\mu_s^2}\sqrt{1-\mu_\gamma^2}\cos(\phi_s-\phi_\gamma), \tag{11}$$

where $\phi_s-\phi_\gamma$ is the difference between the azimuths of the projectile and gamma ray.

We use a Monte-Carlo simulation to calculate the energy distribution of the gamma rays. The distribution of E is determined by the total cross section as a function of energy and the energy spectrum of the primary particles.

The distribution of μ_s^* is determined by the differential cross section in the c.m. frame. At low energies ($\leqslant$ 10 MeV), where resonances occur, there are rapid variations of the angular shapes, but on the average the distributions are close to isotropic. At higher energies, the differential cross sections are more and more peaked in the forward direction, and hence the excited nuclei are emitted preferentially backward with respect to the direction of the incoming protons. In order to account for these effects, we evaluate the differential cross sections in 4 different regions of energy. Below 12 MeV we assume an isotropic distribution; between 12 and 20 MeV we use the data of Peelle (1957) at 15 MeV; between 20 and 60 MeV we adopt the measurements of Dickens et al. (1963) at 28 MeV; and above 60 MeV we use the measurements of Strauch and Titus (1956) at 96 MeV. All these data are for $^{12}C(p,p')^{12}C^{*}4.44$ reactions. By examining the corresponding data for the reaction $^{16}O(p,p)^{16}O^{*}6.13$

(Kobayashi 1960, Daehnick 1964, and Austin et al. 1971) we conclude that, on the average, the shape of the differential cross section of this reaction is almost the same as that of the $^{12}C(p,p')^{12}C^{*4.44}$ reaction.

By using a random number generator to evaluate E and μ_s^*, we can now calculate, from equations (4), (5), (6) and (8), the energy of the excited nucleus. The energy of the gamma ray then follows from equations (9) and (10), where we assume an isotropic distribution of the gamma rays in the rest frame of the emitting nucleus. The cosine of the angle between the gamma ray and the projectile, μ, can now be calculated by using equations (7) and (11), where we assume a uniformly distributed random number for $\phi_s-\phi_\gamma$. The knowledge of μ is required only if the projectile velocities are anisotropic. For isotropic distributions all the gamma rays generated by the simulation contribute to the spectrum, regardless of the value of μ. However, by imposing conditions on μ the effects of anisotropic distributions can be taken into account. For example if the projectile velocities are uniformly distributed in the hemisphere away from the observer, only gamma rays with $-1\leq\mu\leq 0$ contribute to the spectrum, while if the projectiles are confined to the opposite hemisphere, $0\leq\mu\leq 1$. Hereafter these anisotropic distributions will be referred to as the down and up cases, respectively.

In calculating the shape of the gamma-ray lines from the spallation processes of Table 1, we use the same techniques as for the direct excitation processes, except for the following modifications. The Lorentz factor γ_s^* is no longer a unique function of the incident energy E, but can have any value up to a maximum

$$\gamma_s^* \leq \gamma_m^* = (E_{cm}^2 + m_3^2 - m_4^2)/(2\, m_3 E_{cm}), \qquad (12)$$

where m_3 is now the mass, including the excitation energy, of the excited nucleus and m_4 is the sum of the masses of all the other particles that emerge from the reaction. Since there is no data on the distributions of γ_s^* and μ_s^* for these reactions, we have made certain assumptions which lead to a gamma-ray spectrum consistent with the observations of Goryachev et al. (1974) who have resolved the 6.32-MeV line of ^{15}N in the bombardment of ^{16}O with 1 GeV protons. The relatively narrow observed width of this line in the 1 GeV experiment cannot be due to gamma-ray emission from nuclei stopped by the target material, because the lifetime of the 6.32-MeV level in ^{15}N is very short ($<4\times10^{-14}$ sec, De Meijer, Plendl and Holub 1974). The observations of Goryachev et al. (1974), therefore, imply that the ^{15}N nuclei are produced with very low velocities in the laboratory frame. This behavior can be simulated by using the same angular distributions for the multibody spallation reactions as for the 2-body direct excitation processes and by imposing the additional constraints that $\gamma_s^* = \gamma_m^*$ for $\gamma_s^* < \gamma_c$ and $\gamma_s^* = \gamma_c$ for $\gamma_s^* \geq \gamma_c$. Similar assumptions were made by Ramaty and Lingenfelter (1969) and Ramaty and Kozlovsky (1974) for ^3He production in multibody processes resulting from proton-alpha particle reactions in which very low energy ^3He nuclei were produced.

In addition to the narrow lines discussed above, broad gamma-ray lines are produced by the interactions of energetic C, N and O nuclei with ambient H and He. For the evaluation of the shapes of these lines we use the same formulae as for the narrow lines with some modifications. In the 2-body processes m_1 is replaced by m_2 in equation (4), and μ_s^* is replaced $-\mu_s^*$ in equations (6) and (7); in the 3-body processes the excited nucleus is assumed to move with the velocity of the center of mass, $\beta_c = \sqrt{\gamma_c^2 - 1}/\gamma_c$.

Using the above kinematics and nuclear data, and assuming that the H:He:C:N:O ratios of the energetic particles are the same as those of the ambient medium, we have evaluated the gamma-ray spectrum due to both the narrow and broad components. In Figure 6 we show the results for isotropic particle distributions with energy spectra characterized by (s=4, E_c=0), (s=2, E_c=0) and (s=2, E_c=100 MeV/amu). As can be seen, for steep particle spectra (s=4) the most prominent lines are at 4.44 and 6.13 MeV, while for flat spectra (s=2), the spallation lines at 6.32 and $\sim$ 5.2 MeV also become quite noticeable.

The full widths at half maximum (FWHM) of the 4.44 and 6.13 MeV lines are summarized in Table 2. For s=4 the FWHM's are significantly larger than for the other cases because for steep particle spectra the lines are produced predominantly in alpha particle interactions in which the excited nuclei have larger recoil velocities than in proton interactions. The FWHM's, however, do not depend strongly on the energies of the primary particles. For s=2 the width of the 4.44 MeV line, for example, is essentially independent of the cutoff energy E_c. For all three values of E_c shown in Table 2, this line is predominantly due to proton induced interactions. As the energy of the primary proton increases, the c.m. angular distributions of the excited nuclei become more and more peaked in the backward direction. As a result, these nuclei acquire only small recoil velocities even if the energies of the primary protons are large. A similar result would hold for the 6.129-MeV line, except that for E_c = 100 MeV, this line is effectively broadened into a feature of FWHM $\simeq$ 120 keV by the contribution of the 6.17-MeV spallation line.

Another noteworthy feature of the gamma-ray spectra from alpha particle induced interactions (s=4 in Figure 6) is the presence of broad features in addition to narrow lines. In particular, the feature at 4.4 MeV, due to the interactions of energetic C nuclei with ambient helium, has a FWHM of only 500 keV, and hence can be considered as an identifiable broad gamma-ray line. The absence of such a feature in gamma-ray spectra resulting from flat particle spectra is due to the higher average energies at which proton interactions take place, and due to the fact that in interactions with protons the energetic nuclei suffer less energy loss than in interactions with helium nuclei.

In Figure 7 we show results for anisotropic particle distributions. As pointed out by Ramaty and Crannell (1976), if the charged particles are confined to a hemisphere either away (down) or toward (up) the observer there should be a Doppler shift of the mean energy of the lines. We also obtain such shifts; however, since we have taken into account the angular distributions of the excited nuclei in the c.m. frames of the reactions, we find that the shifts are smaller than those given by Ramaty and Crannell (1976) who have assumed isotropic angular distributions. For the 6.129 MeV line, we find in the down case red shifts of about 15 to 20 keV for accelerated particles with s=2 and a shift of about 30 keV for s=4. For the 4.44 MeV line we obtain red shifts smaller by almost a factor of 2. We conclude that such shifts can only be detected with high resolution detectors and sufficient counting statistics.

In addition to the shifts of the mean energies of the narrow lines, anisotropic particle distributions also cause detectable differences in the shapes of the broad lines which appear as underlying continuum in Figure 7. As we shall see in Section IV below, these differences can be

studied by comparing the calculated and observed pulse-height spectra from the solar flare of 1972, August 4.

IV. Discussion and Comparisons with Data

We proceed now to compare the results of our calculations with observational data from the flare of 1972, August 4. Gamma-ray lines were detected from this flare by Chupp et al. (1973, 1975). The detector was flown on OSO-7 satellite and has been described in detail by Higbie et al. (1973).

1. Comparisons of Pulse-Height Spectra

Figures 8 and 9 show comparisons of the observed pulse-height spectrum in the energy range from 4 to 8 MeV with calculated pulse-height spectra. The solid lines represent the pulse-height spectrum from the solar flare obtained by subtracting the antisolar quadrant counting rates from those in the solar quadrant. The dashed lines represent the calculated pulse-height spectrum obtained by folding the gamma-ray spectra of Figures 6 and 7 through the detector response. The folding technique is discussed in the Appendix. The absolute normalizations of the calculated spectra was determined by minimizing the values of χ^2 given by

$$\chi^2 = \Sigma_{i=1}^{15}(C_i^{obs}-C_i^{calc})^2/C_1^{calc}, \qquad (13)$$

where C_i^{obs} and C_i^{calc} are the observed and calculated count rates in 200 keV bins as shown in Figures 8 and 9. The resultant minimal χ^2's are also given in these figures. It is evident from Figure 8 that the calculated spectrum for s=4 gives a poor fit to the data. (The possibility that $\chi^2 = 37.6$ by chance is less than 0.001). Much better fits are provided by the spectra for s=2, E_c=0 and s=2, E_c=100 MeV. By considering Figures 6 and 8 we see that the poor fit for s=4 is caused by the excessive number of photons around 4.4 MeV. As discussed in Section III, these

photons are due to the broad feature at 4.4 MeV produced by (α,α') reactions. As we shall see below, steep particle spectra can also be ruled out from considerations based on the ratio of the 4 to 8 MeV gamma ray intensity to the 2.2-MeV line intensity.

In Figure 9 we compare the data with calculated spectra from particles with different angular distributions. We see that the isotropic and up cases give a better fit to the data than does the down case. The isotropic and up cases are consistent with models wherein the charged particles are accelerated in a second stage mechanism by upward moving shock waves (Wild, Smerd and Weiss 1963, Frost and Dennis 1971, Sturrock 1974, Bai and Ramaty 1976), whereas the down case would correspond to models in which the gamma rays are produced by accelerated particles moving downwards into the photosphere. Unfortunately the data is not sufficiently accurate to completely rule out models in which the particles are beamed downwards.

A further examination of Figures 8 and 9 reveals that the best agreements between the observed and calculated spectra are obtained with particle spectra that are flat at low energies (E_c=30 and 100 MeV/amu). For such spectra there is a large contirbution from spallation reactions which produce the strong line at 6.32 MeV. This line can account, in part, for the observed counts in the 6.2 to 6.4 MeV bin. We should caution, however, that at least some of the observed counts in this bin could be due to 6 to 6.2 MeV photons which were shifted into the next higher bin due to the nonlinearity of the relationship between photon energy and pulse height, and perhaps due to a slight gain shift of the detector's electronic system.

2. Total 4 to 8 MeV Photon Fluxes

We proceed now to evaluate the implications of the total number of photons in the 4 to 8 MeV region. As discussed above, these photons are produced both as narrow lines due to proton and alpha particle interactions, and as broad lines caused by the reactions of energetic C, N and O nuclei. For the compositions used above (H:He:C:N:O = 10^4:10^3:3.7:1.2:6.8 for both accelerated particles and ambient medium) the total 4 to 8 MeV photon production rate is given by

$$Q_{4-8} = 2(q_p+q_\alpha), \tag{14}$$

where q_p and q_α are plotted in Figure 5. However, some of the solar abundances, in particular that of He in both the energetic particles and the ambient medium, are not very well known. If we take these abundances as free parameters, then equation (14) is modified as follows

$$Q_{4-8} = q_p[1+20.4(\alpha/p)]+10q_\alpha[1+20.4(He/H)](\alpha/p), \tag{15}$$

where α/p and He/H are the He to H ratios in the energetic particles and the ambient medium, respectively. It is also assumed in equation (15) that in the energetic particles the C to N to O ratios are the same as those of the ambient medium and that He/(C+N+O) = 42 (Webber et al. 1975).

We have evaluated equation (15) for several values of He/H and α/p. The range $0.07 \leqslant He/H \leqslant 0.1$ is consistent with recent measurements (Brown and Lockman 1975), while the range $0.02 \leqslant \alpha/p \leqslant 0.1$ takes into account most of the observed variation of this ratio for solar flares. In Figure 10 we plot Q_{4-8} as a function of s and E_c for He/H = 0.1 and α/p = 0.05, and in Table 3 we show the variation of Q_{4-8} with He/H and α/p for two extreme

particle spectra. From Table 3 we see that Q_{4-8} can vary by about a factor of 2 for very flat spectra, and by about a factor of 5 for very steep spectra. The significance of these variations will become apparent below, when we compare the ratio of the 4 to 8 MeV photon flux with the 2.2-MeV flux.

The 2.2-MeV line is due to neutron capture by protons. Ramaty et al. (1975) have presented detailed calculations of neutron and 2.2-MeV gamma-ray production in flares. Using their compiled cross sections, we have evaluated the production rate of neutrons, Q_n, for the accelerated particle spectra and compositions discussed above. The results are given in Figure 11 for $\alpha/p = 0.05$ and He/H = 0.1. The variation of Q_n with α/p and He/H is summarized in Table 3. The variation of Q_n with α/p and He/H is of about the same magnitude as that of Q_{4-8}. The ratio Q_{4-8}/Q_n, therefore is almost independent of these parameters. From the neutron production rates, Q_n, given in Figure 11 we evaluate the 2.2-MeV gamma-ray production rate, $Q_{2.2}$, by using the neutron-to-gamma efficiencies, $\bar{f}$, given by Ramaty et al. (1975, figure 9). The ratio $Q_{4-8}/Q_{2.2}$ is plotted in Figure 12 as a function of s and E_c for $\alpha/p = 0.05$ and He/H = 0.1. From the analysis of the Appendix, the observed 4 to 8 MeV photon flux for the 1972, August 4 flare was 0.19 ± 0.02 photons $cm^{-2}s^{-1}$, while the observed 2.2-MeV flux was 0.28 ± 0.02 photons $cm^{-2}s^{-1}$ (Chupp et al. 1975). These values lead to an observed ratio of 0.68 ± 0.1 which is shown by the shaded area in Figure 12.

By comparing the observed and calculated ratios of the 4-8 MeV flux to the 2.2-MeV line flux, we can obtain information on the spectrum of the charged particles. Before considering this comparison, however, let us discuss the principal sources of uncertainty in the calculations leading to the results of Figure 12.

The error in the nuclear cross sections can be estimated from the paper of Zobel et al. (1968) who give errors of less than 20% for the most important lines. Since we consider the sum of the lines in the 4 to 8 MeV range and since the total cross sections for most of these lines are taken from Zobel et al. (1968), we feel that the upper limit on the error due to nuclear cross sections probably does not exceed about 20%.

The uncertainties resulting from compositional variation can be assessed from Table 3. We see that whereas for a given spectrum, Q_{4-8} and Q_n can both vary by up to a factor of 5, the ratio Q_{4-8}/Q_n does not vary by more than 20% when α/p and He/H are allowed to change over their full assumed range of variability. Compositional uncertainties therefore, also do not lead to large errors in $Q_{4-8}/Q_{2.2}$.

Another source of error in the evaluation of $Q_{2.2}$ is the abundance of ^{3}He in the photosphere (Wang and Ramaty 1974). Our calculations are based on $^3He/H = 5x10^{-5}$, a value close to that measured in the solar wind. By decreasing $^3He/H$ arbitrarily to zero, $Q_{4-8}/Q_{2.2}$ is increased by only less than a factor of 2. On the other hand, it is unlikely that the photospheric abundance of ^{3}He is much higher than the solar wind value, since the ^{3}He abundance has now been measured in prominences (Hall 1975), and its value there is close to that detected in the solar wind. We conclude that the photospheric ^{3}He abundance is also not a major source of error in the calculation of $Q_{4-8}/Q_{2.2}$.

Potentially, the largest source of error in the determination of $Q_{4-8}/Q_{2.2}$ is the assumed angular distribution of the neutrons which produce the 2.2-MeV line. This angular distribution should resemble that of the primary charged particles. Our calculations of $Q_{2.2}$ are based on an

isotropic angular distribution. If the neutrons move preferentially downward toward the photosphere, the conversion efficiency, $\bar{f}$, is increased by about a factor of 2, and $Q_{4-8}/Q_{2.2}$ decreases accordingly. If, however, the neutrons move preferentially upward, $\bar{f}$ can be decreased by a large factor and hence $Q_{4-8}/Q_{2.2}$ is increased by the same factor.

In summary, we find that the values of $Q_{4-8}/Q_{2.2}$ could possibly be smaller than those given in Figure 12, but by not more than a factor of about 2. They could, however, be significantly larger, owing mainly to the possibility that the neutrons are preferentially moving away from the photosphere.

By considering now the results of Figure 12, we see that steep particle spectra are inconsistent with the data. The same conclusion has been reached earlier from the comparison of the observed and calculated pulse-height spectra. This conclusion is unmitigated by the above uncertainties because the lowering of $Q_{4-8}/Q_{2.2}$ by about a factor of 2 allows only slightly steeper spectra to become consistent with the data. The increase of $Q_{4-8}/Q_{2.2}$ due to the possible anisotropy of the neutrons leads to flatter spectra than those deduced from the nominal conditions of Figure 12. In fact, because of this uncertainty in $Q_{4-8}/Q_{2.2}$, most values of s with E_c = 100 MeV/amu are probably consistent with the observed 4-8 MeV to 2.2 MeV line ratio, and, furthermore, the values of s deduced for other E_c's should be considered as upper limits only.

For particle spectra with $E_c \leqslant 10$ MeV/amu, the best value of s is about 1.9, whereas for E_c = 30 MeV/amu, s $\simeq$ 2.5. We cannot deduce a value for s for E_c = 100 MeV/amu, but, as we have just discussed, this case can also be consistent with the data provided that the neutron-to-gamma

conversion efficiency is smaller by about a factor of 2 to 5 than the value given by Ramaty et al. (1975) for isotropic particle distributions.

For particle spectra which remain unbroken power laws down to energies less than the gamma-ray production threshold energy ($E_c = 0$), we can set a stringent upper limit on the value of s. If we allow a maximum uncertainty of a factor of 2 in the calculated value of $Q_{4-8}/Q_{2.2}$, then for $E_c = 0$, s should be smaller than 2.5. As we have seen above (Figure 8), s = 4 with E_c = o gives a very poor fit to the observed pulse-height spectrum.

Finally, we can estimate the product of the ambient hydrogen density and the total number of protons of energies greater than 30 MeV, nN_p(>30 MeV). From the observed 4 to 8 MeV gamma-ray flux of 0.19 photons $cm^{-2}sec^{-1}$, $nN_p(>30) \simeq 6x10^{43} cm^{-3}$, for the nominal cases given above (s = 1.9, E_c = o and s = 2.5, E_c = 30 MeV/amu). However, since the E_c = 100 MeV/amu case can also give a fit to the data, nN_p(>30 MeV) could be as large as $2x10^{44} cm^{-3}$. These numbers are in good agreement with those given by Ramaty et al. (1975) who have calculated nN_p on the basis of the narrow lines alone.

In summary, the results of sections IV.1 and IV.2 are that flat particle spectra give a much better fit to the observed gamma-ray spectrum that do steep spectra, that steep spectra produce more total radiation in the 4 to 8 MeV band than observed, and that the entire observed radiation in the 4 to 8 MeV band is probably of nuclear origin in the form of broad and narrow gamma-ray lines.

3. Upper Limits on the Relativistic Electron-to-Proton Ratio in Flares

The implication of the last conclusion given above is that an upper limit can be set on the ratio of genuine continuum to line (both broad and

narrow) emissions in the 4 to 8 MeV energy band. This limit, in turn, sets limits on the proton-to-electron ratio. In the discussion below, we take into account bremsstrahlung only. The inclusion of other radiation mechanisms (which, however, make only very minor contributions) will only lower the deduced e/p limit.

In Figure 13 we show the ratio of the differential proton number to the differential electron number at 10 MeV, $N_p(10)/N_e(10)$, derived so that the total amount of bremsstrahlung in the 4 to 7 MeV range equals Q_{4-8}. It is also assumed that the ambient densities in the interaction regions of the nuclei and the electrons are the same. As can be seen, for a wide range of spectral parameters, solar flares accelerate protons to energies around 10 MeV much more efficiently than they accelerate electrons to similar energies. Bai and Ramaty (1976) have arrived at the same conclusion. Furthermore, these authors have argued that relativistic electrons and nuclei of energies $\geq$ 1 MeV are accelerated in solar flares by a different mechanism than that which accelerates lower energy ($\leq$100 keV) particles. The flare mechanism which accelerates particles to high energies must accelerate protons more efficiently than electrons. We should mention that the accelerator of galactic cosmic rays should have the same property: as for solar flare particles, the ratio of protons to electrons in galactic cosmic rays is around 100 (e.g. Meyer, Ramaty and Webber 1974).

V. Conclusions

We have evaluated in detail the production of nuclear gamma rays in the 4 to 8 MeV region. The radiation in this energy band is due to both narrow lines, produced in the interaction of energetic protons and alpha particles with ambient material, mostly C and O, and to broad lines

resulting from the interactions of energetic C and O nuclei with ambient H and He.

We have studied in detail the nuclear processes which lead to line emissions. We find that the 4 to 8 MeV band has the unique property that it contains almost all the nuclear radiation of the abundant elements C and O, but does not receive significant contributions from other nuclei. This band shows strong lines at 4.44 MeV from ^{12}C and ^{11}B, at 6.13 MeV from ^{16}O, at 6.32 MeV from ^{15}N, and at ~5.2 MeV from ^{15}N and ^{15}O. The 6.13 MeV line is produced by direct excitation reactions, the 4.44 MeV line is produced by both direct excitation and spallation reactions, and the 6.32 and 5.2 MeV lines are due to spallation reactions only. Spallation reactions, in general, make a strong contribution to the gamma-ray spectrum only if the charged particles have flat energy spectra.

The FWHM's of the narrow lines are almost independent of the energies of the primary particles. The FWHM's of the 4.44-MeV and 6.13-MeV lines are about 45 keV and 65 keV respectively, if excited by protons, and larger by about a factor of 2, if excited by alpha particles. Since for steep particle spectra, most of the gamma rays are produced by alpha particle induced reactions, the widths of the lines for such spectra are significantly larger than the widths obtained for flat spectra.

Thus, the widths of the lines as well as the presence or absence of lines from spallation reactions could give information on the energy spectrum of the accelerated particles.

The gamma-ray spectrum is also affected by the angular distribution of the accelerated charged particles. For example, if the particles have velocity vectors confined to a hemisphere either towards or away from the observer, the narrow lines are shifted upwards or downwards in energy.

The shift of the mean energy of the 6.13-MeV line, however, is only about 15 keV, a value too small to be resolved by present detectors. The shift of the 4.44-MeV line is even smaller. On the other hand, the broad lines undergo much larger shifts which lead to modifications in the gamma-ray spectra that are observable even with presently available instrumentation.

We have folded the calculated gamma-ray spectra through the response function of the University of New Hampshire gamma-ray detector flown on OSO-7. By comparing the calculated and observed pulse-height spectra, we conclude that the entire 4 to 8 MeV spectrum can be attributed to nuclear radiation, that flat particle spectra produce gamma-ray spectra which fit the data much better than those produced by steep spectra, and that the data is better fit if the particles have isotropic or upward-moving angular distributions than if the particles' velocity vectors are confined to the downward hemisphere. Since the 1972, August 4 flare was close to the sub-Earth point on the Sun, the upward or downward hemispheres correspond to those toward or away from the observer.

Information on the spectrum of the accelerated particles can also be obtained by comparing the total nuclear radiation in the 4 to 8 MeV region with the 2.2-MeV line intensity observed from solar flares. We find that the spectral index of the differential particle number in the 10 to 100 MeV/amu range cannot be larger than 2.5, since for steeper spectra the 4 to 8 MeV band would contain more radiation than observed. This result takes into account uncertainties due to the composition of both the accelerated particles and the ambient medium, and the abundance of ^{3}He in the photosphere. It is not possible, however, to set a lower limit on the spectral index. Even though very flat spectra produce an overabundance of

neutrons relative to 4 to 8 MeV photons, this overabundance does not necessarily lead to an overabundance of 2.2-MeV gamma rays, since the neutron-to-gamma-ray conversion efficiency decreases with increasing upward anisotropy of the accelerated particles. This anisotropy could be studied by measuring simultaneously the fluxes of 2.2-MeV gamma-rays and solar neutrons.

The fact that essentially all the observed radiation in the 4 to 8 MeV region from the solar flare of 1972, August 4 is of nuclear origin, sets upper limits on the electron-to-proton ratio in flares. We find that at 10 MeV, the ratio between the differential number of electrons to protons cannot exceed about 0.05.

Acknowledgments

We wish to thank Professor E. L. Chupp for providing the OSO-7 gamma ray data. Part of the research of A.N.S. was supported by Goddard contract NAS5-11276 at the University of New Hampshire.

VI. Appendix

It is well known that when monoenergetic photons in the energy range from about 0.2 to 20 MeV are incident on a NaI(Tℓ) detector, the observed pulse-height spectrum consists of a photopeak, Compton continuum and, above 1.022 MeV of two annihalation gamma-ray escape peaks. It is often desirable to convert the observed NaI pulse-height spectrum into the true gamma-ray spectrum or visa versa. The problem of converting a measured pulse-height spectrum into an incident photon spectrum requires detailed information on the detector response function.

The response function of the University of New Hampshire (UNH) gamma-ray detector was measured for gamma-ray energies of 0.393, 0.662, 1.12, 1.37 and 2.75 MeV (Higbie et al. 1973). Above 1 MeV the photopeak sensitivity of the detector can be approximated by the relation

$$S_{ph} = 10.1\ \varepsilon^{-0.807}\ \text{counts cm}^2/\text{photon}, \tag{16}$$

where ε is the energy of the photon in MeV. We have extrapolated this relation to the 4-8 MeV range because there is no experimental data above 2.75 MeV. When a flux F of gamma rays of energy ε is incident on the detector for a time t it causes a photopeak in the observed spectrum; the number of events in this peak is given by

$$N_{ph} = S_{ph} F\ t. \tag{17}$$

The UNH gamma-ray detector is shielded by a thick CsI(Na) shield. The anticoincidence action of the shield reduces the contributions

of the Compton continuum and the annihilation gamma-ray escape peaks by a factor about 1.5. As a result of the suppression of the escape peaks, the area under the second escape peak in the energy range 4 to 8 MeV is negligible. For the UNH gamma-ray detector the ratio between the area under the first escape peak and the photopeak was measured at 2.75 and 6.13 MeV. Experimental data (Heath 1964) and the Monte-Carlo calculations of Berger and Seltzer (1972) show that this ratio is a linear function of the gamma-ray energy in the energy range 2 to 8 MeV. We have, therefore, used the following relation in the energy range 4 to 8 MeV,

$$N_{es}/N_{ph} = 0.08\varepsilon - 0.135, \qquad (18)$$

where N_{es} is the number of counts in the first escape peak.

Measured pulse-height spectra for gamma-ray energies of 0.66, 1.12, 1.37 and 2.75 MeV were used to calculate the experimental values of the peak-to-total ratio (N_{ph}/N_T). Here N_T is the total number of counts in the pulse-height spectrum. In the determination of N_T we have approximated the Compton tail and the 'valley fill' function by a single rectangular function. Since no experimental data is available above 2.75 MeV, we have used the Monte-Carlo calculations of Giannini et al. (1970) to construct the peak-to-total ratio curve above 3 MeV. Giannini et al (1970) have calculated the photopeak and the total detection sensitivities for a 7.6cm x 7.6cm NaI crystal for gamma-ray energies up to 10 MeV. The Monte-Carlo calculations of Giannini et al. (1970) were chosen because their calculations give peak-to-total ratios which are in good agreement with the experimental data (e.g. Heath 1964, Misra and Sadasivan 1969). Above 3 MeV, the peak-to total ratio for the UNH gamma-ray detector can be represented by

the relation,

$$N_{ph}/N_T = 0.69\ \varepsilon^{-0.80}. \tag{19}$$

Knowing N_{ph}, N_{es}, and N_T, the number of counts in the Compton continuum is given by

$$N_c = N_T - N_{ph} - N_{es}. \tag{20}$$

The relationship between the energy of a gamma ray and the channel number n of the pulse height analyser is given by a quadratic formula (P. P. Dunphy, private communication 1973)

$$\varepsilon = K(n+n_o)^2, \tag{21}$$

where from ground calibration data $n_o = 80.2$. The value of K can vary due to gain changes in the detector. For the 1972, August 4 flare period the mean value of K was found to 0.393×10^{-4}.

The procedure adopted to convert the calculated photon spectrum in the energy range 4-8 MeV to the pulse-height spectrum is as follows. The energy range 4-8 MeV was divided into bins of 200 keV width each. This bin width is chosen to retain the instrumental resolution width of the detector which is about 140 keV at 5 MeV. All the photons falling in a given energy bin are considered to have the mid-bin energy of that bin. Starting from the highest energy bin, the contribution of the Compton continuum associated with the counts in this bin was determined for all the bins lower than this bin. This procedure was repeated for the second bin and so on down to the last bin. The total Compton contribution for each bin was then determined by summing up the individual contribution from bins higher than that bin. Similarly starting from the highest energy bin and working down, the area under the first escape peak was determined and added to the bin shifted down in energy by

0.51 MeV from the contributing bin. Finally, the expected number of counts in each bin was determined by adding the photopeak, Compton and first escape peak contributions.

It is clear from the foregoing discussion that the counting rate, due to a flux of photons from a gamma-ray spectrum incident on the detector, consists of the sum of contributions from photopeak, first escape peaak and Compton continuum. Using the folding procedure described above, we have converted several calculated gamma-ray spectra into pulse-height spectra. From the comparison of these spectra we find that the relation between the incident flux of 4 to 8 MeV photons (F_{4-8}) and the counting rate (C_R) can be expressed as,

$$C_R = R_F F_{4-8} = 0.106 F_{4-8}. \quad (22)$$

This relation depends only weakly on the spectral shape of the accelerated charged particles. For the particle spectra discussed in this paper, the value of C_R does not change by more than 5% of the value given in equation (22).

The observed pulse-height spectrum for the 1972, August 4 event was accumulated during the time interval of 91.6 sec. The total number of counts observed in this time interval was 82 ± 9. Since the area of the detector is $45 cm^2$, $F_{4-8} = 0.19\pm0.02$. This is the number that we used in Section IV.2.

References

Ajzenberg-Selove, F. and Lauritsen, T., 1968, Nucl. Phys., A114, 1.

Alard, J. P., Baldit, A., Costilhes, J. P., Fargeix, J., Roche, R. and Tamain, J. C., 1975, Nuovo Cimento (Letters), 10, 841.

Austin, S. M., Locard, P. J., Bunder, S. N., Cameron, J. M., Richardson, J. R., Verbal, J. W., Van Oers, W. T. H., 1971, Phys. Rev. C3, 1514.

Bai, T., and Ramaty, R., 1976 Solar Phys. (in press).

Barnard, A. C. L., Swint, J. B. and Clegg, T. B. 1966, Nucl. Phys., 86, 130.

Berger, M. J. and Seltzer, S. M. 1972, Nucl. Instr. Methods, 104, 317.

Bergman, C., and Hobbie, R. K. 1971, Phys. Rev. C3, 1729.

Blatchley, D. E., and Bent, R. D. 1965, Nucl. Phys., 61, 641.

Brown, R. L., and Lockman, F. J. 1975, Ap. J. (Letters), 200, L155.

Cameron, A. G. W. 1973, Space Sci. Rev. 15, 121.

Chupp, E. L., Forrest, D. J., Higbie, P. R., Suri, A. N., Tsai, C. and Dunphy, P. P. 1973, Nature 241, 333.

Chupp, E. L., Forrest, D. J. and Suri, A. N., 1975, in S. Kane (ed.), Solar γ-, X- and EUV Radiation, IAU Symp. 68, p. 341.

Clegg, A. B., Foley, K. J., Salmon, G. L., and Segal, R. E., 1961, Proc. Phys. Soc., 78, 681.

Conzett, H. E., 1957, Phys. Rev., 105, 1324.

Corelli, J. C., Bleuler, E., and Tendam, D. J., 1959, Phys. Rev., 116, 1184.

Crannell, C. J., Joyce, G., Ramaty, R., and Werntz, C., 1976, Ap. J. (in press).

Crawley, G. M. and Garvey, G. T., 1967, Phys. Rev. 160, 981.

Daehnick, W. W., 1964, Phys. Rev. 135, B1168.

Daehnick, W. W. and Sherr, R., 1964, Phys. Rev. 133, B934.

Dangle, R. L., Oppliger, L. D. and Hardie, G. 1964, Phys. Rev. 133, B647.

DeMeijer, R. S., Plendel, H. S., and Holub, R., 1974, Atomic Data and Nucl. Data Tables, 13, 1.

Dickens, J. K., Haner, D. A., Waddell, C. N., 1963, Phys. Rev. 132, 2159.

Emmerson, J. M., Madden, J. C. W., Johnson, C. M. P., Middlemas, N., Clegg, A. B., and Williams, W. S. C., 1966, Nucl. Phys. 77, 305.

Fannon, J. A., Burge, E. J., Smith, D. A., and Ganguly, N. K., 1967, Nucl. Phys., A97, 263

Foley, K. J., Salmon, G. L., and Clegg, A. B., 1962, Nucl. Phys., 31, 43.

Frost, K. J., and Dennis, B. R., 1971, Ap. J., 165, 655.

Giannini, M., Oliva, P. R., and Romorino, M. C., 1970, Nucl. Instr. Methods, 81, 104.

Goryachev, Yu. M., Kanavets, V. P., Kirpichnikov, I. V., Levintov, I. I., Morozov, B. V., Nikiforov, N. A. and Starostin, A. S., 1973, Sov. J. Nucl. Phys., 17, 476.

Hall, D. N. B., 1975, Ap. J., 197, 509.

Harvey, B. G., Meriwether, J. R., Mahoney, J., Bussiere De Nercy, A., Horen, D. J., 1966, Phys. Rev., 146, 712.

Heath, R. L. 1964, Scintillation Spectroscopy, Gamma Ray Spectrum Catalogue, Report No. IDO-16880-1.

Higbie, P. R., Forrest, D. J., Gleske, I. U. and Chupp, E. L. 1973, Nucl. Instr. Methods, 108, 167.

Horowitz, Y. S. and Bell, R. E. 1970, Canad, J. Phys., 48, 204.

Hornyak, W. F. and Sherr, R., 1955, Phys. Rev. 100, 1409.

Kobayashi, S. 1960, J. Phys. Soc. Japan, 15, 1164.

Lingenfelter, R. E. and Ramaty, R., 1967, in B. P. S. Shen (ed.), High Energy Nuclear Reactions Astrophysics, W. A. Benjamin, New York, p. 99.

Lingenfelter, R. E., and Ramaty, R., 1976, Ap. J. (Letters), in press.

Macleod, A. M., and Reid, J. M., 1966, Proc. Phys. Soc., 87, 437.

Meneguzzi, M. and Reeves, H., 1975, Astron. Astrophys., 40, 91.

Meyer, P., Ramaty, R., and Webber, W. R., 1974, Physics Today, 27, 23.

Misra, U. C., and Sadasivan, S. 1969, Nucl. Instr. Methods, 69, 330.

Peelle, R. W., 1957, Phys. Rev. 105, 1311.

Ramaty, R., and Lingenfelter, R. E., 1969, Ap. J., 155, 587.

Ramaty, R., and Kozlovsky, B., 1974, Ap. J. 193, 729.

Ramaty, R., Kozlovsky, B., and Lingenfelter, R. E., 1975, Space Sci. Rev. 18, 341.

Ramaty, R. and Crannell, C. J., 1976, Ap. J., 203, 766.

Reich, C. W., Phillips, G. C. and Russell, J. L., 1956, Phys. Rev. 104, 150.

Stovall, T., and Hintz, M., 1964, Phys. Rev. 135, B330.

Strauch, K., and Titus, F., 1956, Phys. Rev., 103, 200.

Sturrock, P. A. 1974, Coronal Disturbances, IAU Symposium No. 57 (D. Reidel, Dordrecht-Holland), p. 437.

Sundberg, O. and Tibell, G. 1969, Arkiv For Fysik, 39, 397.

Suri, A. N., Chupp, E. L., Forrest, D. J., and Reppin, C., 1975, Solar Phys., 43, 415.

Tyren, H., and Maris, T. A. J., 1957, Nucl. Phys., 4, 637.

Wang, H. T., and Ramaty, R., 1974, Solar Phys., 36, 129.

Webber, W. R., Roelof, E. C., McDonald, F. B., Teegarden, B. J. and Trainor, J. 1975, Ap. J., 199, 482.

Wild, J. P., Smerd, S. F. and Weiss, A. A. 1963, Ann. Rev. Astron. Astrophys., 1, 291.

Zobel, W., Maienschein, F. C., Todd, J. H. and Chapman, G. T., 1968, Nucl. Sic. and Eng. 32, 392.

Table 1

Prompt gamma ray lines in the energy range 4 to 8 MeV

Photon Energy (MeV)	Emission Mechanism	Production Processes
4.438	$^{12}C^{*4.439} \rightarrow$ g.s.	$^{12}C(p,p')^{12}C^*$ $^{12}C(\alpha,\alpha')^{12}C^*$ $^{16}O(p,\ )^{12}C^*$ $^{14}N(p,\ )^{12}C^*$
4.443	$^{11}B^{*4.444}$	$^{12}C(p,2p)^{11}B^*$ $^{12}C(\alpha,\ )^{11}B^*$ $^{16}O(p,\ )^{11}B^*$ $^{14}N(p\ )^{11}B^*$
5.180	$^{15}O^{*5.181} \rightarrow$ g.s.	$^{16}O(p,pn)^{15}O^*$
5.241	$^{15}O^{*5.242} \rightarrow$ g.s.	$^{16}O(\alpha,\ )^{15}O^*$
5.270	$^{15}N^{*5.271} \rightarrow$ g.s.	$^{16}O(p,2p)^{15}N^*$
5.298	$^{15}N^{*5.299} \rightarrow$ g.s.	$^{16}O(\alpha,\ )^{15}N^*$
6.129	$^{16}O^{*6.131} \rightarrow$ g.s.	$^{16}O(p,p')^{16}O^*$ $^{16}O(\alpha,\alpha')^{16}O^*$
6.176	$^{15}O^{*6.177} \rightarrow$ g.s.	$^{16}O(p,pn)^{15}O^*$ $^{16}O(\alpha\ )^{15}O^*$
6.322	$^{15}N^{*6.324} \rightarrow$ g.s.	$^{16}O(p,2p)^{15}N^*$ $^{16}O(\alpha,\ )^{15}N^*$
6.337	$^{11}C^{*6.339} \rightarrow$ g.s.	$^{12}C(p,pn)^{11}C^*$
6.478	$^{11}C^{*6.480} \rightarrow$ g.s.	$^{12}C(p,pn)^{11}C^*$
6.741	$^{11}B^{*6.743} \rightarrow$ g.s.	$^{12}C(p,2p)^{11}B^*$
6.791	$^{11}B^{*6.793} \rightarrow$ g.s.	$^{12}C(p,2p)^{11}B^*$
6.917	$^{16}O^{*6.919} \rightarrow$ g.s.	$^{16}O(p,p')^{16}O^*$ $^{16}O(\alpha,\alpha')^{16}O^*$
7.117	$^{16}O^{*7.119} \rightarrow$ g.s.	$^{16}O(p,p')^{16}O^*$ $^{16}O\ \alpha,\alpha')^{16}O^*$

Table 2

Line Widths of 4.44 and 6.13 MeV Lines

S	E_c (MeV/amu)	FWHM (keV) 4.44 MeV	6.13 MeV
4	0	110	140
2	0	45	65
2	30	45	65
2	100	50	120

Table 3

Selected 4-8 MeV Production Rates (photons sec^{-1} $Hatom^{-1}$) and Neutron Production Rates (neutrons sec^{-1} $Hatom^{-1}$)

	He/H = 0.07		He/H = 0.1		
α/p	Q_{4-8}	Q_n	Q_{4-8}	Q_n	
0.02	2.37×10^{-18}	1.18×10^{-16}	2.38×10^{-18}	1.39×10^{-16}	S = 1.5, E_c = 30 MeV/amu
0.05	3.44×10^{-18}	1.43×10^{-16}	3.47×10^{-18}	1.63×10^{-16}	S = 1.5, E_c = 30 MeV/amu
0.1	5.23×10^{-18}	1.83×10^{-16}	5.29×10^{-18}	2.03×10^{-18}	S = 1.5, E_c = 30 MeV/amu
0.02	1.66×10^{-15}	0.92×10^{-15}	1.97×10^{-15}	1.14×10^{-15}	S = 5, E_c = 0
0.05	3.68×10^{-15}	2.12×10^{-15}	4.55×10^{-15}	2.65×10^{-15}	S = 5, E_c = 0
0.1	7.04×10^{-15}	4.11×10^{-15}	8.57×10^{-15}	5.16×10^{-15}	S = 5, E_c = 0

Figure Captions

1. Production cross sections for the 4.44 MeV line from ^{12}C. Closed data points - proton induced reactions; open point - alpha particle induced reactions.
2. Production cross sections for gamma-ray lines from spallation reactions on ^{16}O. Closed points - 4.44 MeV gamma rays; open points - 5.2 MeV gamma rays. The dashed-dotted line is the sum of the cross sections for the production of the 6.322 and 6.176 MeV lines.
3. Cross sections for line production in the 6.1-6.3 MeV range from ^{16}O.
4. Production cross sections for the 2.74, 6.92 and 7.12 MeV gamma-ray lines from ^{16}O.
5. Production rates of narrow gamma-ray lines in the 4 to 8 MeV region. The sum of the production rates of the narrow lines due to proton (q_p) and alpha (q_α) particle interactions are also shown in this figure.
6. Calculated gamma-ray spectra resulting from accelerated charged particles with isotropic angular distribution.
7. Calculated gamma-ray spectra resulting from anisotropic particle distributions with energy spectrum characterized by $s = 2$ and $E_c = 30$ MeV/amu.
8. Comparison of the observed pulse-height spectrum from the flare of 1972, August 4 with the calculated pulse-height spectra obtained from the gamma-ray spectra shown in Figure 6. We limit the comparison to the 4-7 MeV range because there were no observed counts above 7 MeV.

9. Comparison of the observed pulse-height spectrum from the flare of 1972, August 4, with the calculated pulse-height spectra resulting from the gamma-ray spectra shown in Figure 7.

10. Q_{4-8} as a function of s and E_c, where Q_{4-8} is the production rate of photons in the 4 to 8 MeV energy interval. These production rates are normalized so that for all values of E_c, including E_c = 100 MeV/amu, the number of protons with energies greater than 30 MeV is unity.

11. Q_n as a function of s and E_c, where Q_n is the production rate of of neutrons. The normalization of the rates is the same as that in Figure 10.

12. The $Q_{4-8}/Q_{2.2}$ ratio, where $Q_{2.2}$ is the production rate of 2.2-MeV gamma rays from neutron capture. The shaded area represent the observed ratio of photons in the 4 to 8 MeV range to the observed photons in the 2.2 MeV line.

13. $N_p(10)/N_e(10)$ as a function of the spectral index (Se) of the accelerated electrons. $N_p(10)$ and $N_e(10)$ are the differential numbers of protons and electrons at 10 MeV respectively.

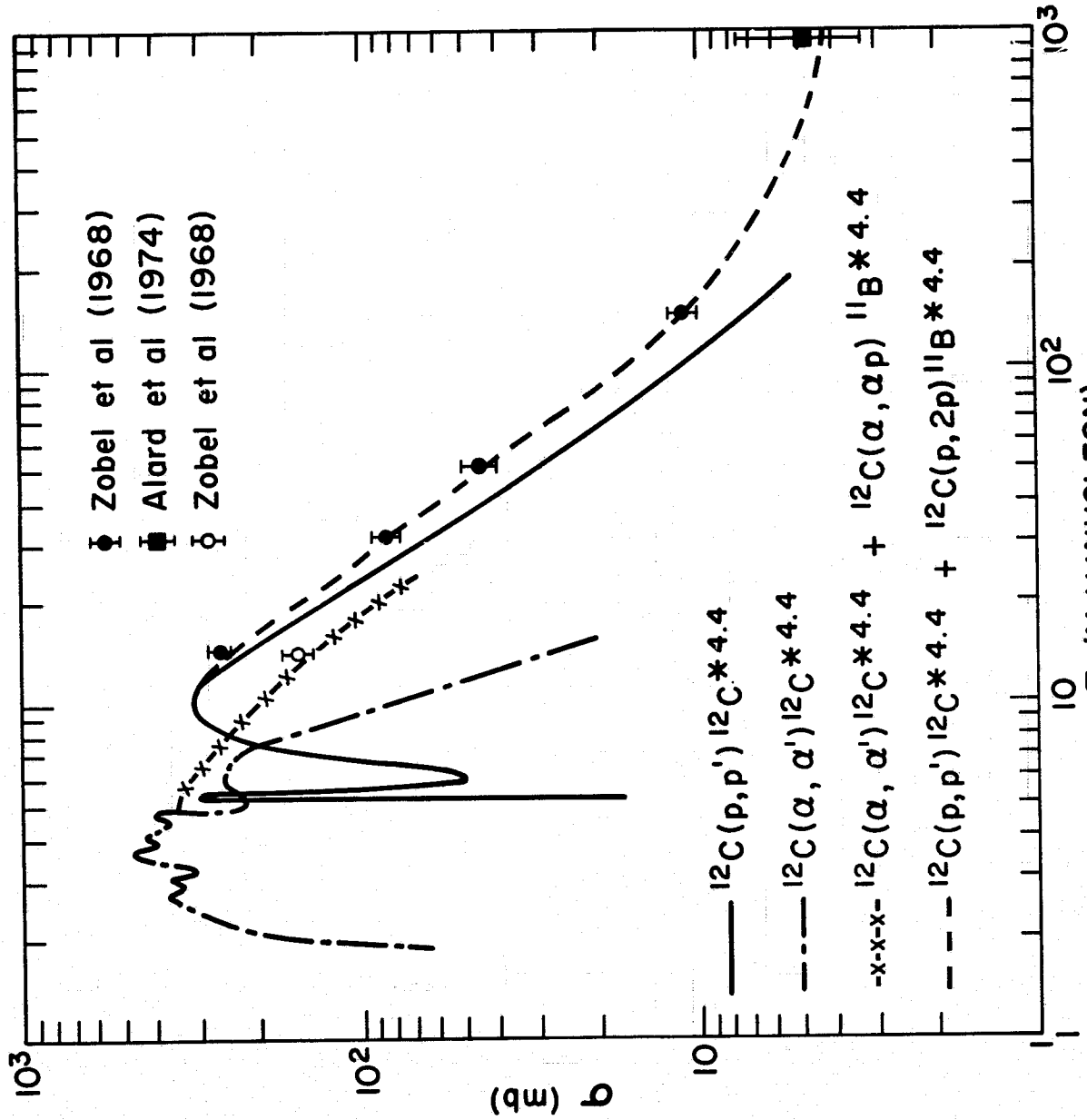

Fig. 1

PRECEDING PAGE BLANK NOT FILMED

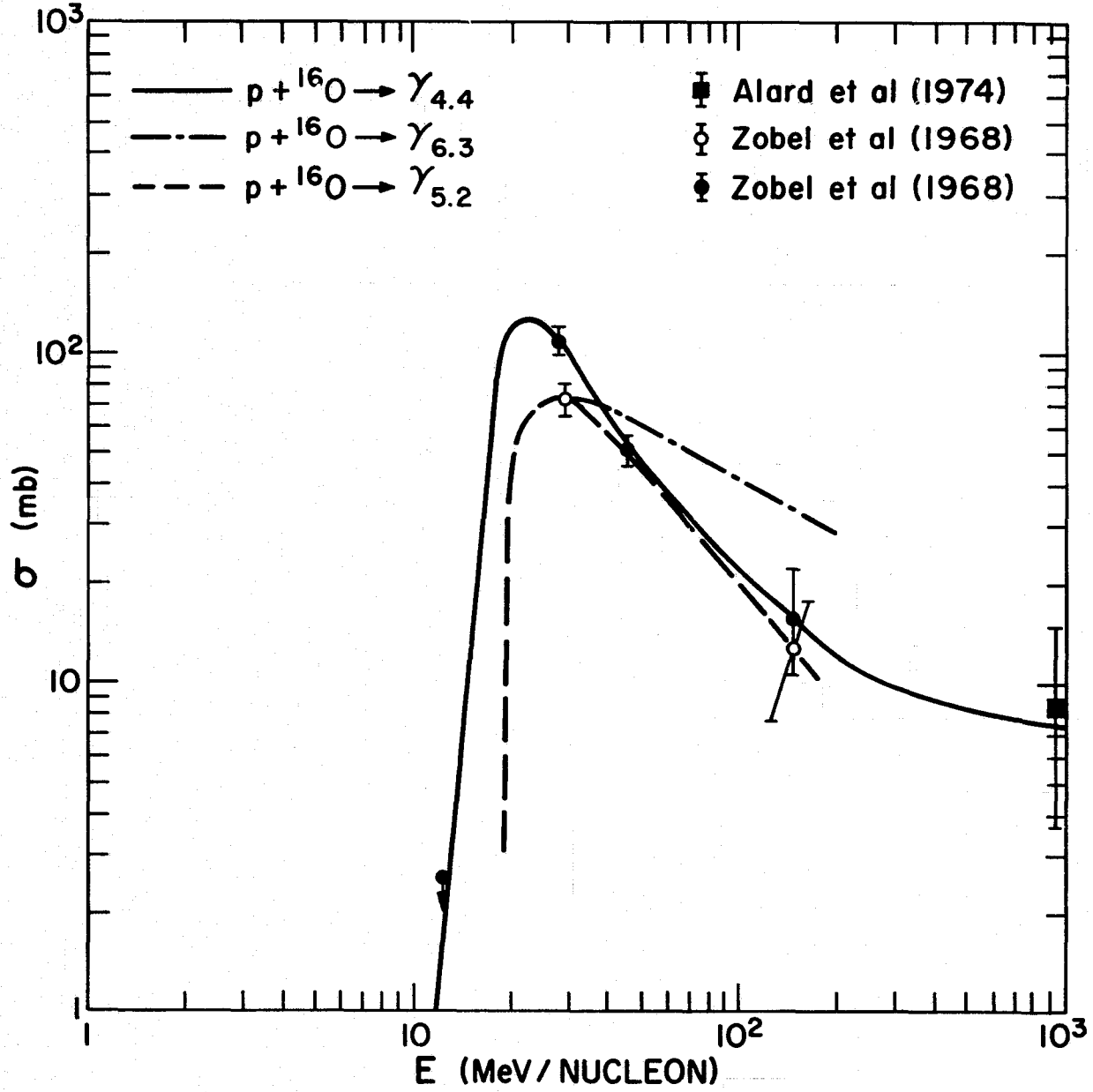
$p + {}^{16}O \rightarrow \gamma_{4.4}$
$p + {}^{16}O \rightarrow \gamma_{6.3}$
$p + {}^{16}O \rightarrow \gamma_{5.2}$
Alard et al (1974)
Zobel et al (1968)
Zobel et al (1968)
10^3
10^2
10
1
σ (mb)
1
10
10^2
10^3
E (MeV / NUCLEON)

Fig. 2

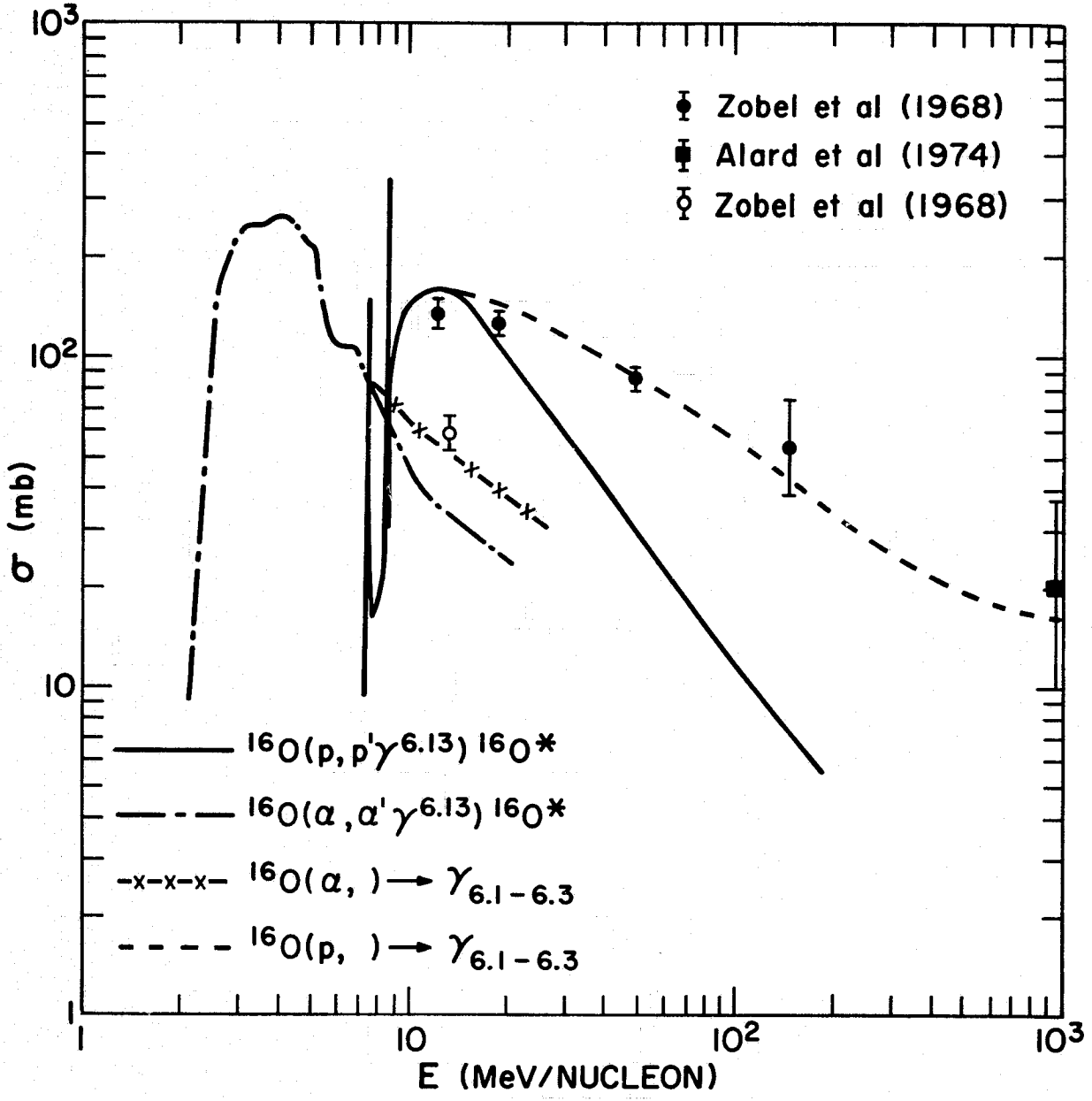
Zobel et al (1968)
Alard et al (1974)
Zobel et al (1968)
σ (mb)
E (MeV/NUCLEON)
$^{16}O(p,p'\gamma^{6.13})\,^{16}O^*$
$^{16}O(\alpha,\alpha'\gamma^{6.13})\,^{16}O^*$
$^{16}O(\alpha,\ ) \rightarrow \gamma_{6.1-6.3}$
$^{16}O(p,\ ) \rightarrow \gamma_{6.1-6.3}$

Fig. 3

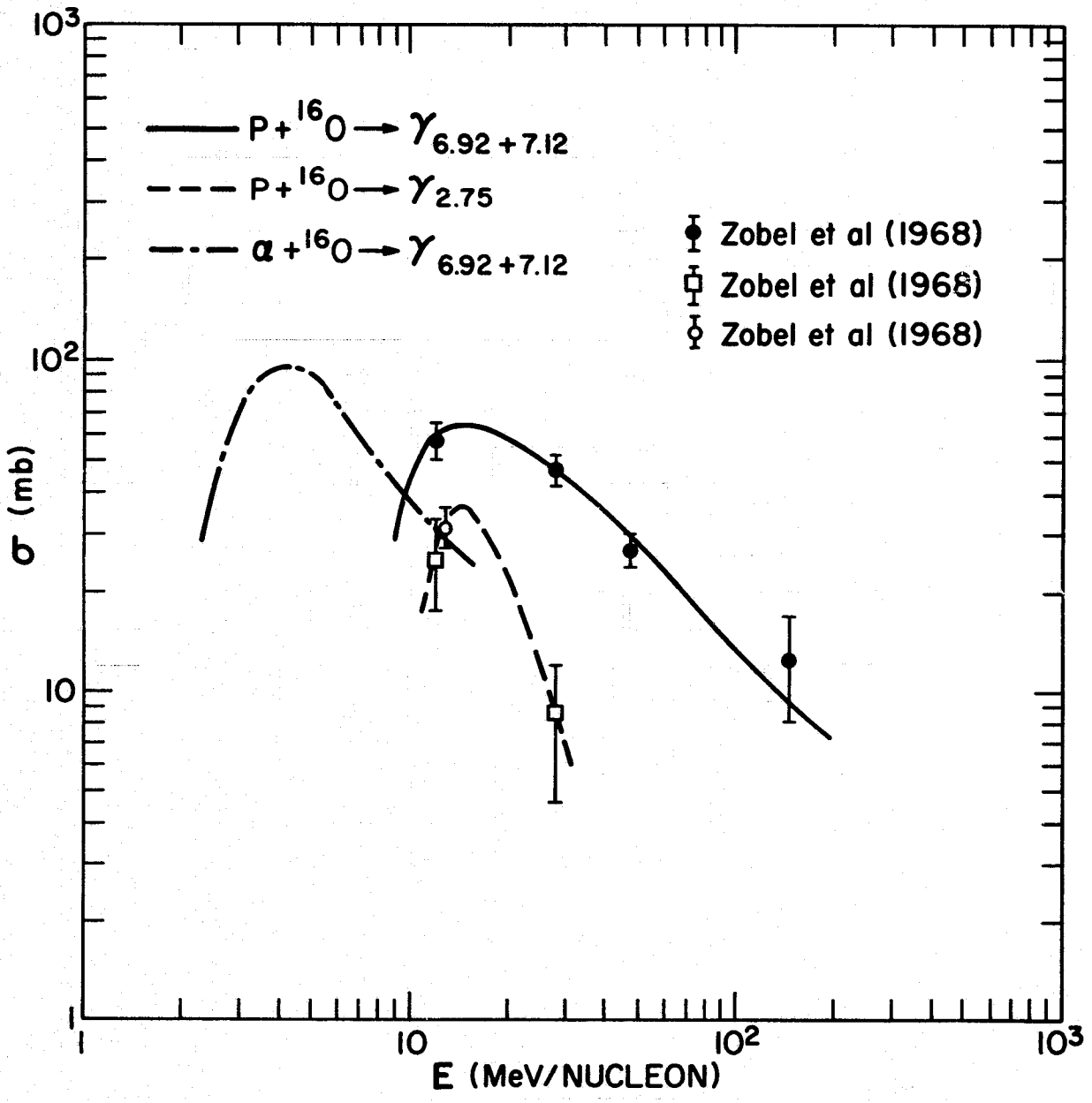
10^3
10^2
10
1
$P + {}^{16}O \rightarrow \gamma_{6.92+7.12}$
$P + {}^{16}O \rightarrow \gamma_{2.75}$
$\alpha + {}^{16}O \rightarrow \gamma_{6.92+7.12}$
Zobel et al (1968)
Zobel et al (1968)
Zobel et al (1968)
σ (mb)
1
10
10^2
10^3
E (MeV/NUCLEON)

Fig. 4

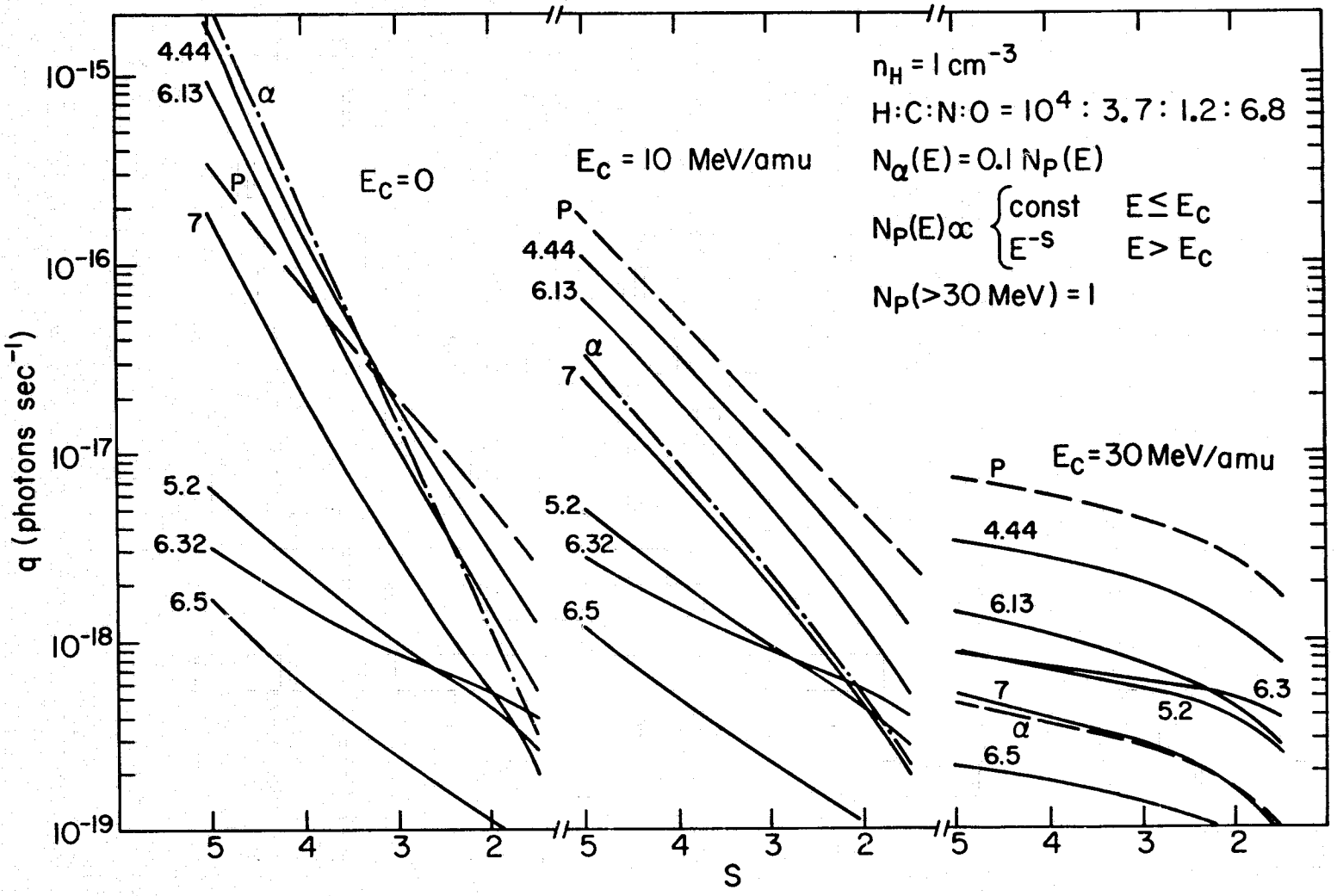
$n_H = 1\ cm^{-3}$
H:C:N:O = 10^4 : 3.7 : 1.2 : 6.8
$N_\alpha(E) = 0.1\ N_P(E)$
$N_P(E) \propto \begin{cases} \text{const} & E \le E_C \\ E^{-s} & E > E_C \end{cases}$
$N_P(>30\ MeV) = 1$
$E_C = 0$
$E_C = 10$ MeV/amu
$E_C = 30$ MeV/amu
q (photons sec^{-1})
S
P
α
4.44
6.13
7
5.2
6.32
6.5
6.3
10^{-15}
10^{-16}
10^{-17}
10^{-18}
10^{-19}
5
4
3
2

Fig. 5

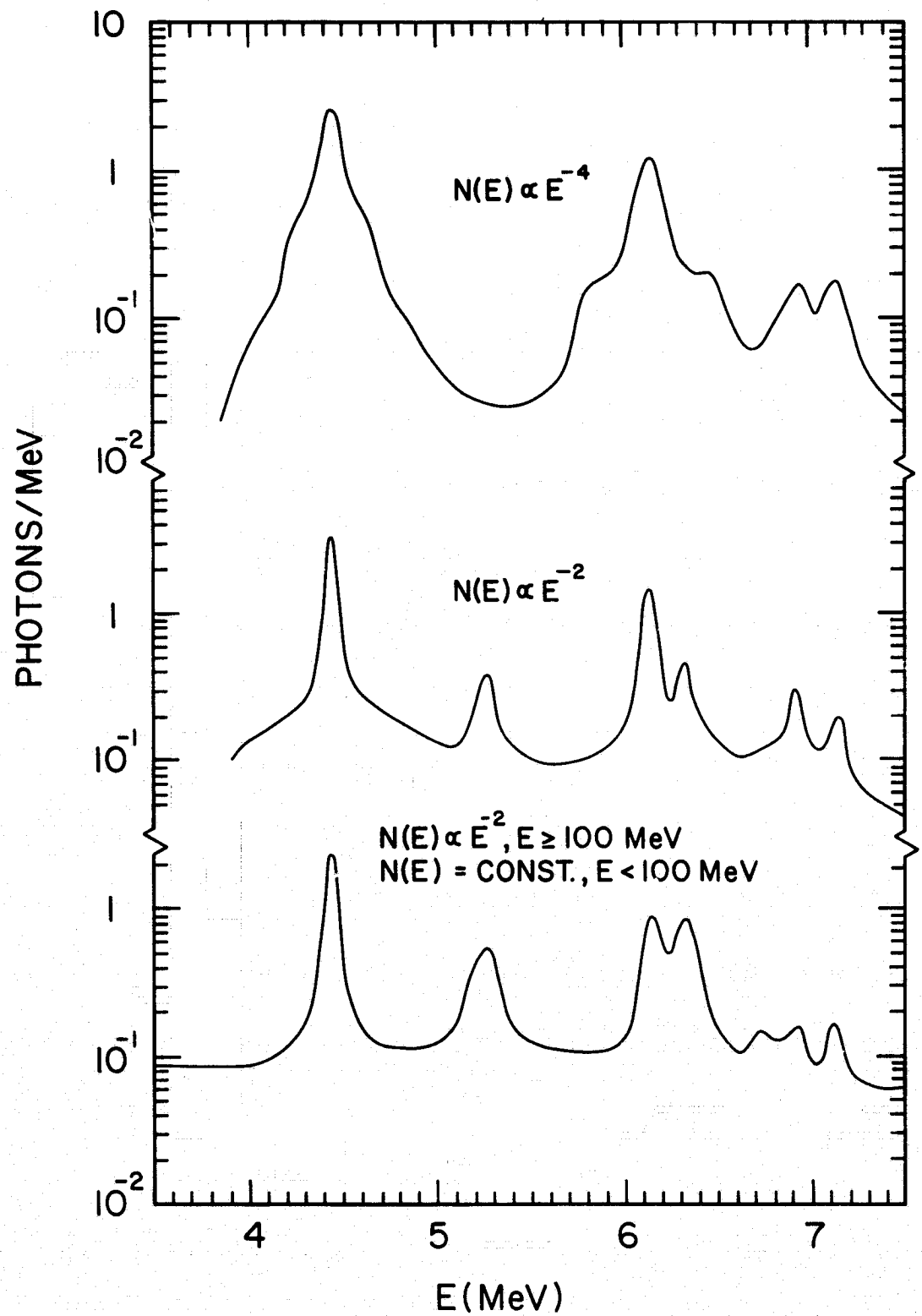
10
1
10^{-1}
10^{-2}
PHOTONS/MeV
$N(E) \propto E^{-4}$
$N(E) \propto E^{-2}$
$N(E) \propto E^{-2}$, $E \geq 100$ MeV
$N(E) = CONST.$, $E < 100$ MeV
4
5
6
7
E(MeV)

Fig. 6

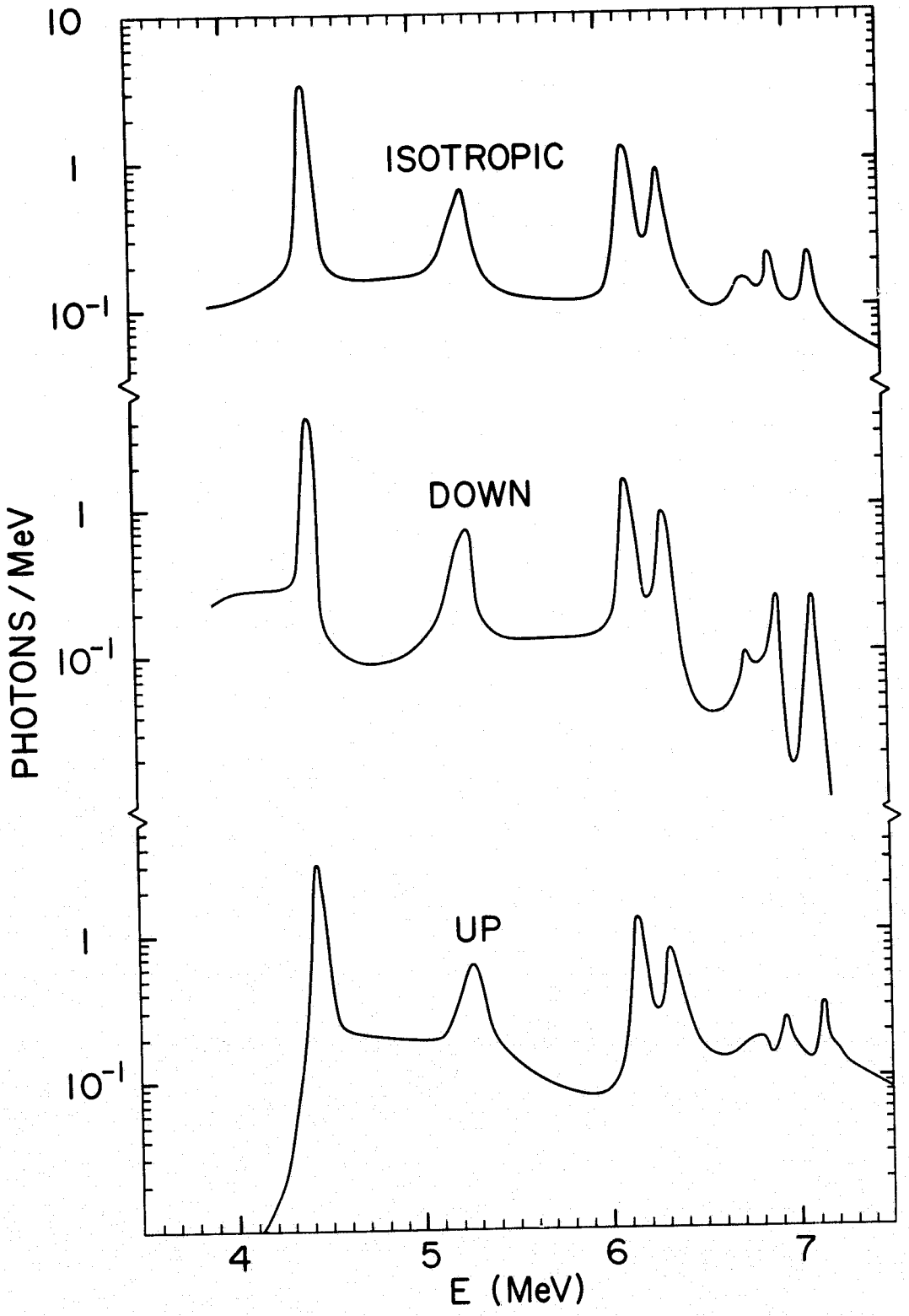

Fig. 7

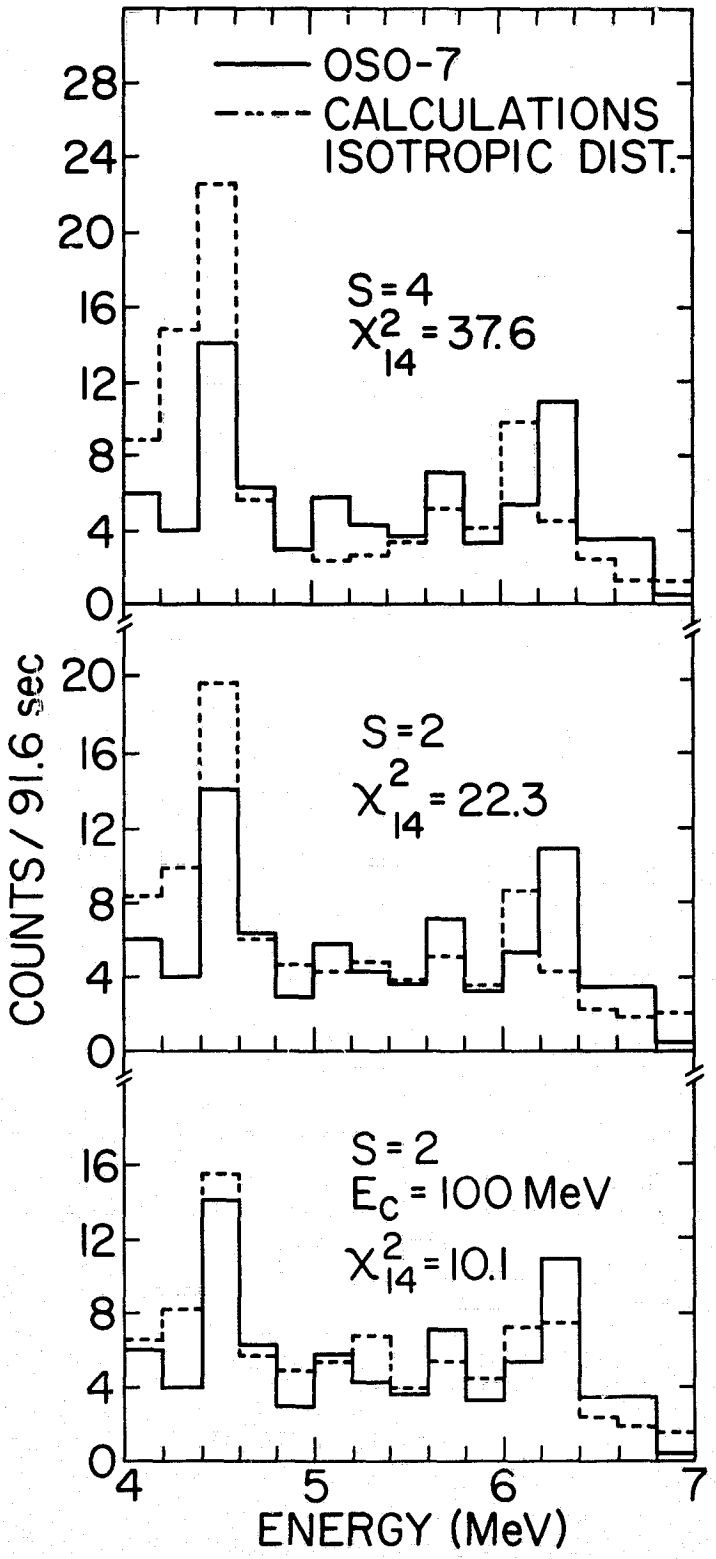
OSO-7
CALCULATIONS
ISOTROPIC DIST.
S=4
X^2_{14}=37.6
S=2
X^2_{14}=22.3
S=2
E_C=100 MeV
X^2_{14}=10.1
COUNTS/91.6 sec
ENERGY (MeV)

Fig. 8

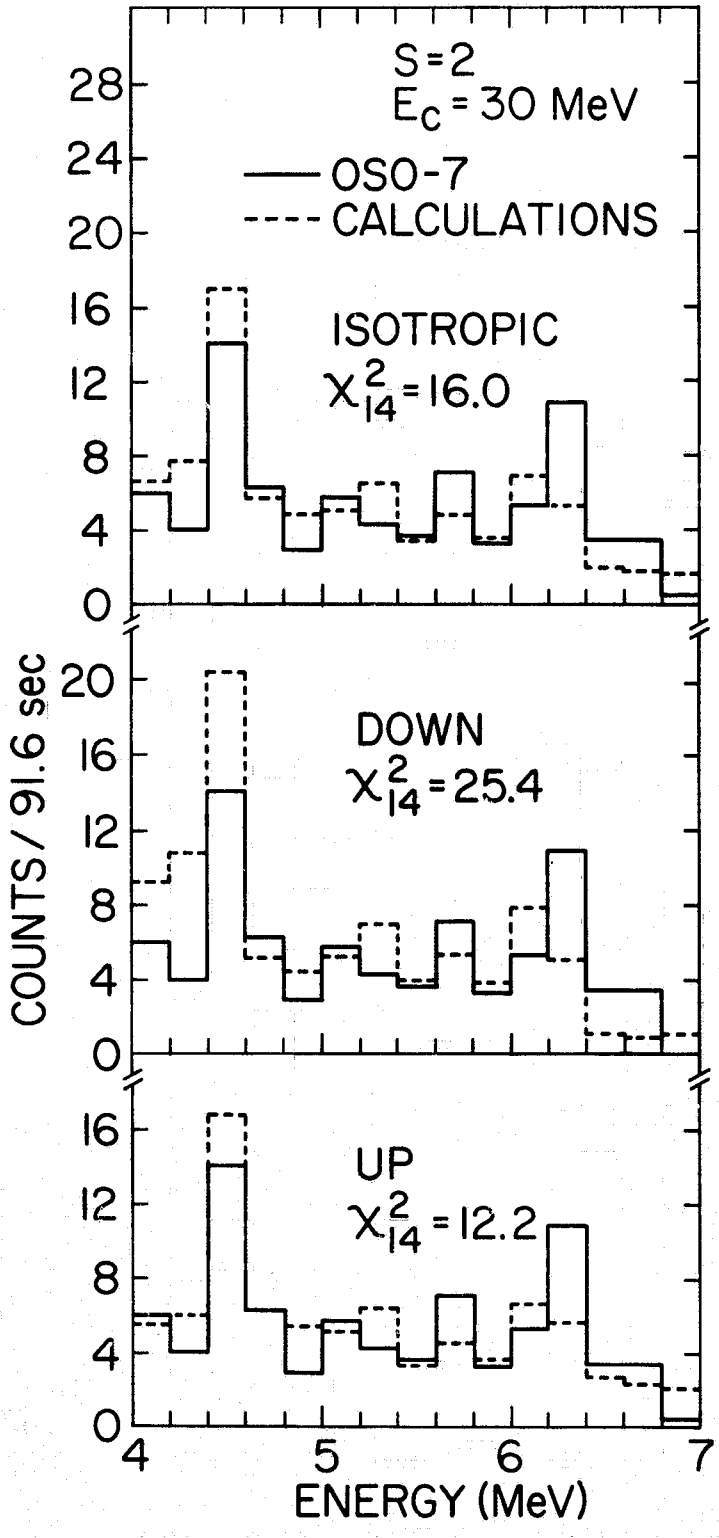
S=2
E_c = 30 MeV
OSO-7
CALCULATIONS
ISOTROPIC
χ^2_{14}=16.0
DOWN
χ^2_{14}=25.4
UP
χ^2_{14}=12.2
COUNTS / 91.6 sec
ENERGY (MeV)

Fig. 9

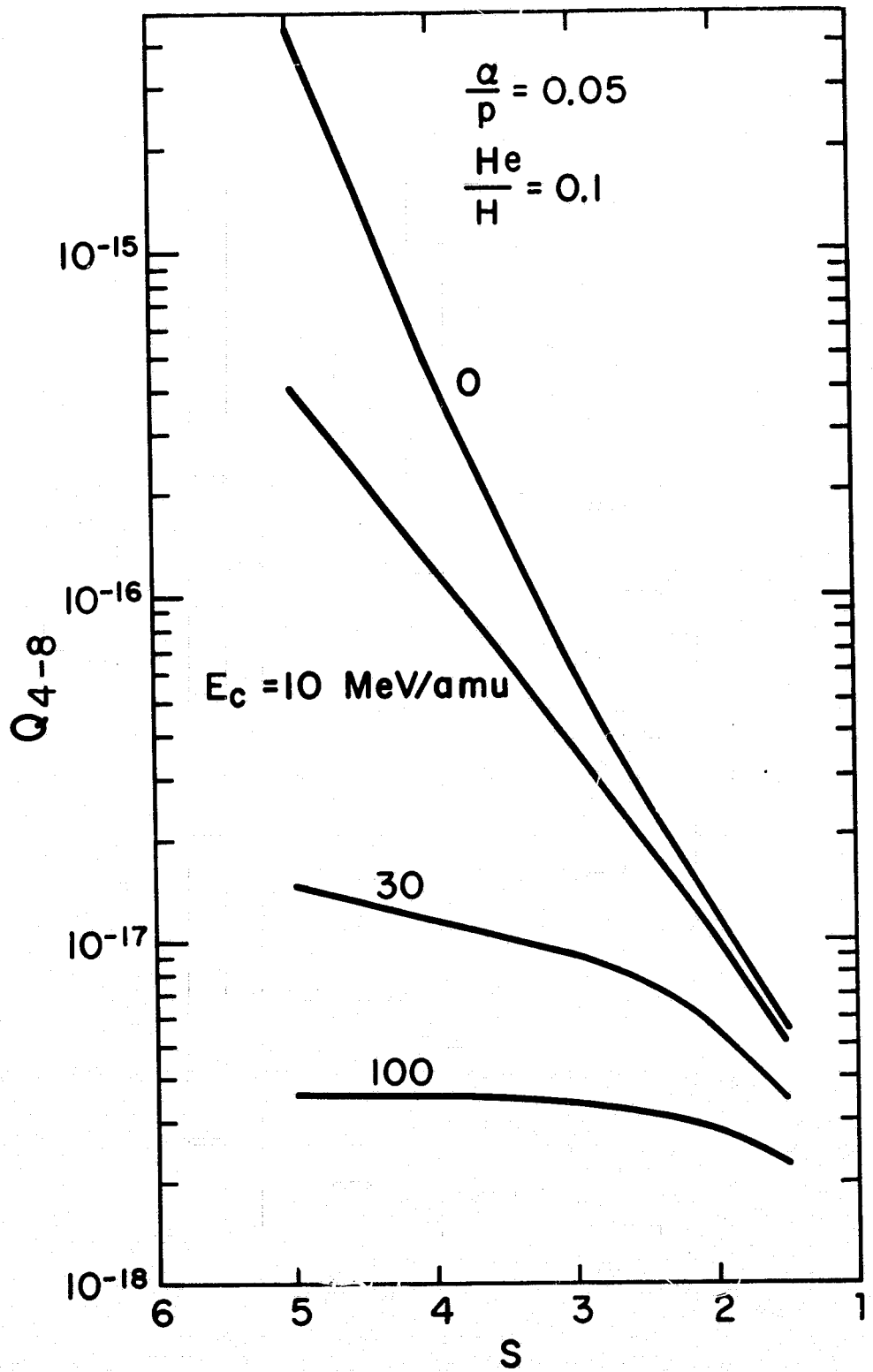
α/p = 0.05
He/H = 0.1
0
30
100
Ec =10 MeV/amu
Q4-8
10-15
10-16
10-17
10-18
6
5
4
3
2
1
S

Fig. 10

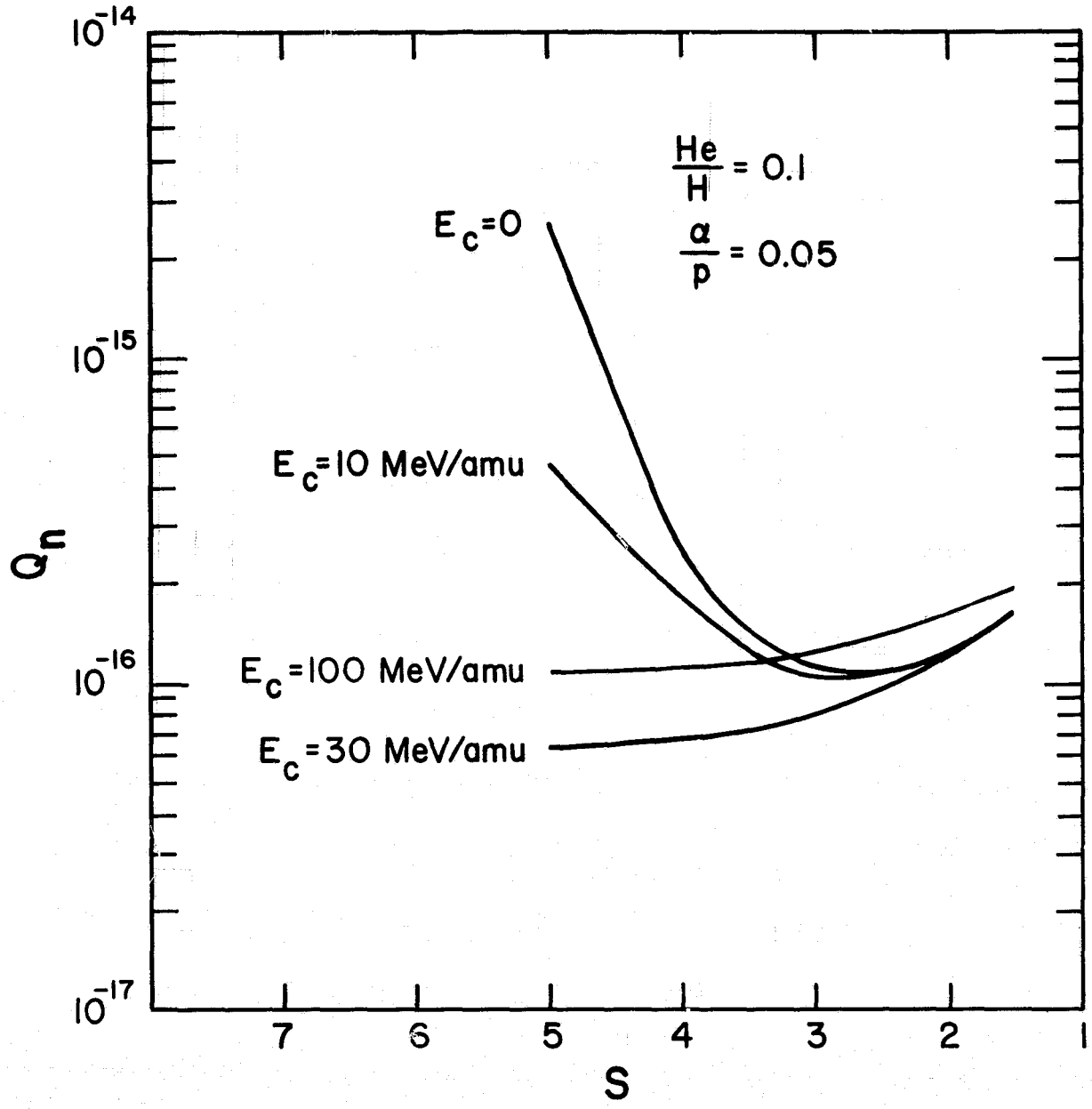
10^{-14}
10^{-15}
10^{-16}
10^{-17}
Q_n
$\frac{He}{H} = 0.1$
$\frac{\alpha}{p} = 0.05$
$E_c = 0$
$E_c = 10$ MeV/amu
$E_c = 100$ MeV/amu
$E_c = 30$ MeV/amu
7
6
5
4
3
2
1
S

Fig. 11

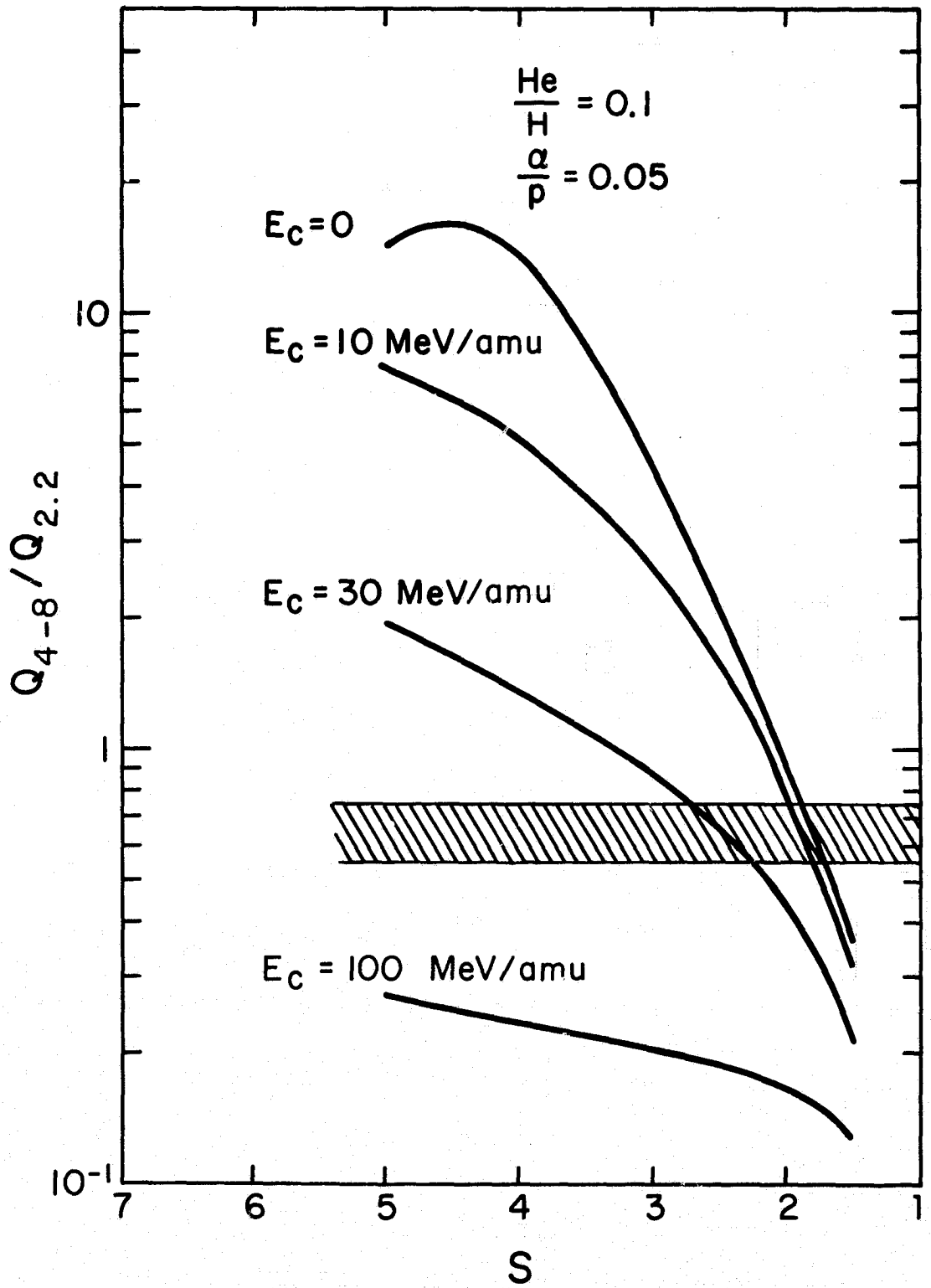
He/H = 0.1
α/p = 0.05
Ec=0
Ec = 10 MeV/amu
Ec = 30 MeV/amu
Ec = 100 MeV/amu
Q4-8/Q2.2
10
1
10-1
7
6
5
4
3
2
1
S

Fig. 12

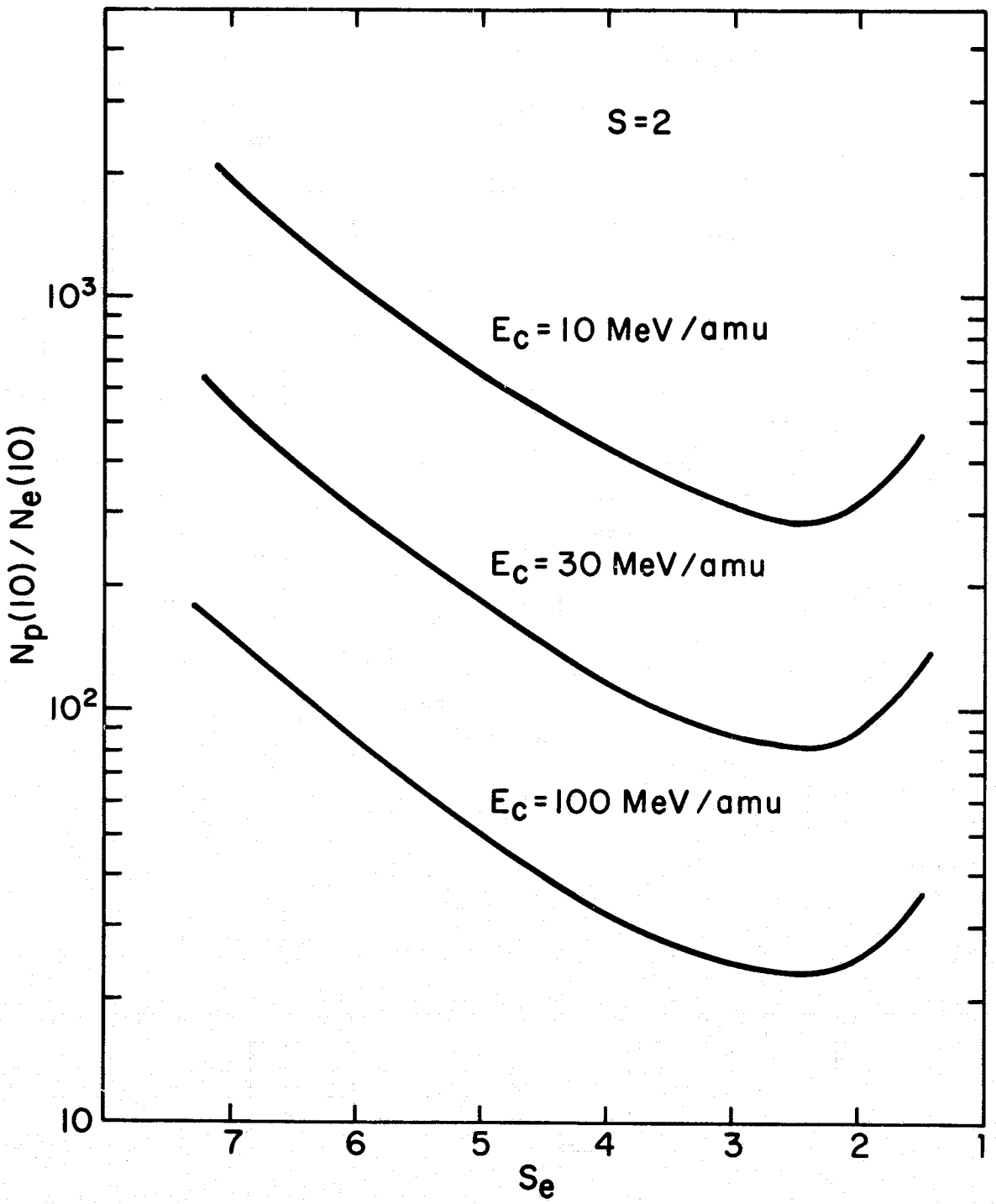
S=2
E_c = 10 MeV/amu
E_c = 30 MeV/amu
E_c = 100 MeV/amu
$N_p(10)/N_e(10)$
10^3
10^2
10
7
6
5
4
3
2
1
S_e

Fig. 13